

Supporting Information: Size-Independent Energy Transfer in Biomimetic Nanoring Complexes

Patrick Parkinson,^{†,¶,§} Nuntaporn Kamonsutthipajit,^{‡,§} Harry L. Anderson^{*,‡} and Laura M. Herz^{*,†}

[†] Department of Physics, University of Oxford, Clarendon Laboratory, Parks Road, Oxford, OX1 3PU, and [‡] Department of Chemistry, University of Oxford, Chemistry Research Laboratory, 12 Mansfield Road, Oxford, OX1 3TA

Contents

A. General Methods	2
B. Synthetic Procedures	2
B1. Synthesis of known compounds.....	2
B2. Synthesis of free-base dipyriddy-substituted porphyrin dimer (P2py2)	3
5-(3,5-Bis(dodecyloxy)-4-pyridyl)-15-(3,5-bis(trihexylsilyl)phenyl)-porphyrin (1)	3
[5-(3,5-Bis(dodecyloxy)-4-pyridyl)-15-(3,5-bis(trihexylsilyl)-phenyl)-porphyrinato]-zinc(II) (2)	4
[5,15-Dibromo-10-(3,5-bis(dodecyloxy)-4-pyridyl)-20-(3,5-bis(trihexylsilyl)-phenyl)-porphyrinato]-zinc(II) (3)	4
[5-(3,5-Bis(dodecyloxy)-4-pyridyl)-15-(3,5-bis(trihexylsilyl)-phenyl)-10,20-(trihexylsilylethynyl)-porphyrinato]-zinc(II) (4)	4
[5-(3,5-Bis(dodecyloxy)-4-pyridyl)-10-ethynyl-15-(3,5-bis(trihexylsilyl)-phenyl)- 20-(trihexylsilylethynyl)-porphyrinato]-zinc(II) (5)	5
Dimerization of [5-(3,5-bis(dodecyloxy)-4-pyridyl)-10-ethynyl-15-(3,5-bis(trihexylsilyl)-phenyl)-20-(trihexylsilylethynyl)-porphyrinato]-zinc(II) (synthesis of dimer (6), P2py2-Zn)	5
Demetallation of zinc dimer P2py2-Zn (6) (synthesis of free-base dimer (7), P2py2)	6
C. Determination of stoichiometries of complexes	8
C1. ¹H-NMR of c-P6•P2py2 complex to confirm the stoichiometry	9
D. Determination of binding constant, K_f	12
D1. UV/Vis/NIR formation titration	12
D2. UV/Vis/NIR denaturation titration	16
Calculation of the formation constant K_f	20
D3. Determination of reference constants	21
D4. Summary of denaturation and formation constants of nanoring-dimer complexes	24
E. Excitation Wavelength Selection	25
F. Photoluminescence observation of Complex Dissociation	26
G. Experimental Energy Transfer Rates	27
H. The models of nanorings minimized geometries calculated using HyperChem®	27
I. Energy Transfer Models	28

A. General Methods

All chemicals were purchased from commercial suppliers and used without further purification unless otherwise stated. Dry toluene, THF, chloroform and CH₂Cl₂ were obtained by passing through a column of activated alumina under nitrogen pressure. Diisopropylamine (DIPA) was dried over calcium hydride, distilled and stored under nitrogen over molecular sieves (3 Å, 8–12 mesh).

All manipulations of oxygen- or water-sensitive compounds were performed using standard high-vacuum techniques.

Analytical thin-layer chromatography (TLC) was carried out on aluminum-backed silica gel 60 F254 plates. Flash column chromatography was performed on Merck silica gel 60 (40–63 μm). Size exclusion chromatography was carried out on Biobeads SX1 (cross-linked polystyrene) under gravity elution. “Petrol ether” (PE) always refers to 40/60 petrol ether.

¹H and ¹³C NMR spectra were recorded on a Bruker Avance 400 (400.13 and 100.64 MHz), a Bruker DQX 400 (400.13 and 100.64 MHz), a Bruker DRX 500 and Bruker Avance II 500 (500.13 and 125.77 MHz) at 298 K unless otherwise stated. TopSpin (Version 3.1) and Spinworks were used. Chemical shifts (δ in ppm) are referenced to solvent residual peaks (CDCl₃ at δ_H 7.26, δ_C 77.16 and toluene-d₈ at δ_H 2.08, 6.97, 7.01 and 7.09). Abbreviations for ¹H-NMR data: s = singlet, d = doublet, t = triplet, m = multiplet, “t” = pseudo triplet, br = broad. Abbreviations for ¹³C-DEPTQ-NMR data: u = up (CH₃ or CH), d = down (CH₂ or Cq).

MALDI-TOF-MS was measured with a Waters MALDI Micro MX spectrometer. *Trans*-2-[3-(4-tert-butylphenyl)-2-methyl-2-propenylidene]malononitrile (DTCB) was used as a matrix for all MALDI-TOF measurements.

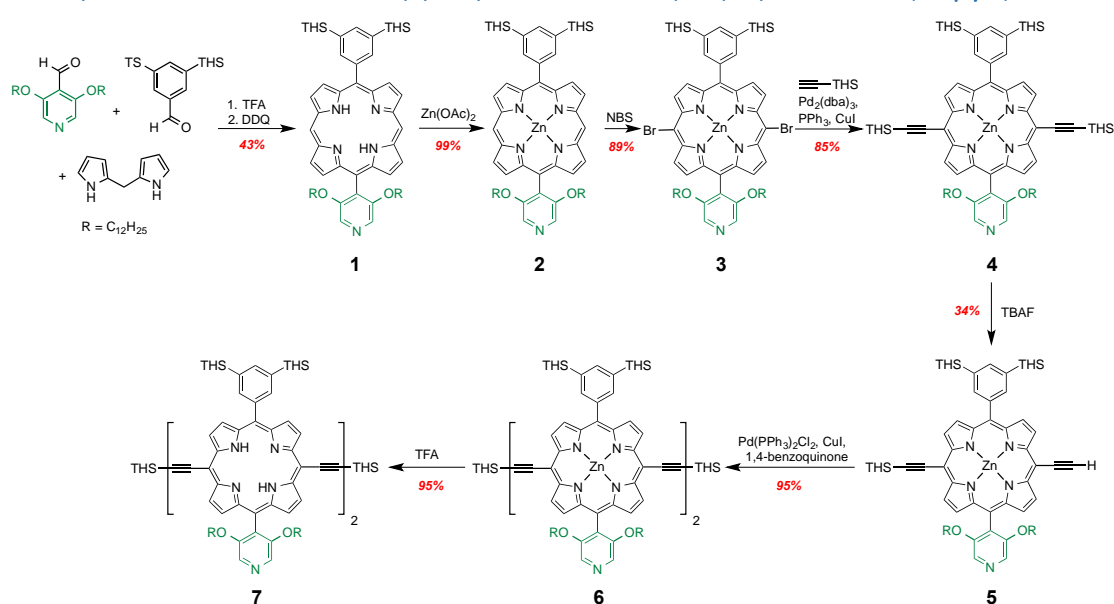
All UV-vis-NIR spectra were recorded at 25 °C on a Perkin-Elmer Lambda 25 photospectrometer using quartz 1 cm cuvettes. The concentration was calculated using the known extinction coefficient of the oligomer. For denaturation titrations, the volume of the ligand required was calculated and added to the cuvette. To this solution, aliquots of a stock solution of pyridine were added. The titrations were performed at a constant temperature of 25 °C, controlled by a thermostat. The curve fitting was carried out using Origin 8.5.1.

B. Synthetic Procedures

B1. Synthesis of known compounds

The porphyrin nanorings were synthesized according to the established procedures using Pd/Cu catalyzed-oxidative coupling of linear porphyrin oligomers with templates.^{1–4}

B2. Synthesis of free-base dipyriddy-substituted porphyrin dimer (P2py2)



Scheme S1: Overview of the synthesis of free-base dipyriddy-substituted porphyrin dimer **P2py2** (THS = Si(C₆H₁₃)₃). The starting aldehydes, 3,5-bis(trihexylsilyl)benzaldehyde and 3,5-bis-(dodecyloxy)isonicotinaldehyde, were synthesized according to ref. [5,6,7], respectively.

5-(3,5-Bis(dodecyloxy)-4-pyridyl)-15-(3,5-bis(trihexylsilyl)phenyl)-porphyrin (**1**)

In a 3 L round-bottom-flask, equipped with a stir bar DCM (1900 mL) (freshly opened bottle) was placed. The flask was sealed with a subaseal and evacuated down to 1 mbar followed by backfilling with nitrogen three times. Light was excluded by wrapping the flask with aluminum foil. 3,5-Bis-(dodecyloxy)isonicotinaldehyde (4.34 g, 9.12 mmol), 3,5-bis-(trihexylsilyl)benzaldehyde (3.10 g, 4.56 mmol) and dipyrrolemethane (2.0 g, 13.68 mmol) were added. The mixture was degassed again as described above. Trifluoroacetic acid (2.20 mL, 28.3 mmol) was added slowly over 5 min under vigorous stirring. The reaction mixture was stirred for 3 h. DDQ (4.66 g, 20.5 mmol) was added and stirring continued for 40 min. Triethylamine (11.4 mL, 82.1 mmol) was added and stirring continued for 30 min. The volume was reduced and the resulting dark solution filtered over a plug of silica eluting with DCM/MeOH (98:2). The solvent was removed from the dark filtrate. The dark residue was dissolved in DCM/MeOH (99:1) and purified by column chromatography (silica, eluent: DCM), resulting in two fractions. The second fraction was collected that contained the desired product. After removal of solvent, this fraction was dissolved in chloroform and precipitated with MeOH, producing compound **1** in the form of a purple oil (2.75 g, 43%).

TLC: *R_f* (DCM) = 0.31; ¹H-NMR (500 MHz, CDCl₃): δ = 10.24 (s, 2H, *meso*-H), 9.33 (d, ³J_{HH} = 4.6 Hz, 2H, β-H), 9.31 (d, ³J_{HH} = 4.5 Hz, 2H, β-H), 9.04 (d, ³J_{HH} = 4.6 Hz, 2H, β-H), 8.91 (d, ³J_{HH} = 4.5 Hz, 2H, β-H), 8.50 (s, 2H, py-H), 8.31 (s, 2H, *o*-H), 7.99 (s, 1H, *p*-H), 3.94 (t, ³J_{HH} = 6.3 Hz, 4H, OCH₂), 1.53-1.44 (m, 12H, CH₂), 1.40-0.70 (m, 96H, CH₂ and CH₃), 0.62-0.54 (m, 4H, CH₂), 0.52-0.34 (m, 12H, CH₂), -3.04 (s, 1H, NH), -3.07 (s, 1H, NH); ¹³C{¹H}-NMR (125 MHz, CDCl₃): δ = 155.6 (2C, py-C), 146.9 (4C, α-C), 145.2 (4C, α-C), 140.9 (2C, *o*-C), 139.5 (1C, *ipso*-C), 139.2 (1C, *p*-C), 135.2 (2C, *m*-C), 131.8 (2C, β-C), 131.1 (2C, β-C), 131.0 (2C, β-C), 130.0 (2C, β-C), 129.1 (2C, py-C), 127.1 (1C, py-C), 120.9 (1C, *meso*-C), 107.6 (1C, *meso*-C), 104.8 (2C, *meso*-C), 69.6 (2C, OCH₂), 33.5 (6C, CH₂), 31.8 (2C, CH₂), 31.6 (6C, CH₂), 29.3 (2C, CH₂), 29.2 (2C, CH₂), 29.1 (2C, CH₂), 29.0 (2C, CH₂), 28.9 (2C, CH₂), 28.5 (2C, CH₂), 28.5 (2C, CH₂), 25.1 (2C, CH₂), 24.0 (6C, CH₂), 22.6 (6C, CH₂), 22.6 (2C, CH₂), 14.1 (6C, CH₃), 14.1 (2C, CH₃), 12.7 (6C, CH₂).

[5-(3,5-Bis(dodecyloxy)-4-pyridyl)-15-(3,5-bis(trihexylsilyl)-phenyl)-porphyrinato]-zinc(II) (2)

A solution of zinc acetate-dihydrate (1.77 g, 9.66 mmol) in MeOH (18.0 mL) was added into a solution of porphyrin **1** (2.75 g, 1.96 mmol) in CHCl₃ (140 mL). The mixture was stirred at 40 °C for 2 h then filtered over a plug of silica, eluting with DCM/pyridine (99:1). The solvent was removed from the pink filtrate and the residue was dried in high vacuum, yielding the desired product **2** (2.84 g, 99%) in the form of a pink, sticky solid.

¹H-NMR (500 MHz, CDCl₃+1% pyridine-*d*₅): δ = 10.08 (s, 2H, *meso*-H), 9.28 (d, ³J_{HH} = 4.4 Hz, 2H, β-H), 9.25 (d, ³J_{HH} = 4.5 Hz, 2H, β-H), 9.02 (d, ³J_{HH} = 4.4 Hz, 2H, β-H), 8.89 (d, ³J_{HH} = 4.4 Hz, 2H, β-H), 8.45 (s, 2H, py-H), 8.30 (s, 2H, *o*-H), 7.95 (s, 1H, *p*-H), 3.86 (t, ³J_{HH} = 6.4 Hz, 4H, OCH₂), 1.51-1.42 (m, 12H, CH₂), 1.38-0.77 (m, 96H, CH₂ and CH₃), 0.71- 0.63 (m, 4H, CH₂), 0.48-0.43 (m, 8H, CH₂), 0.36-0.27 (m, 4H, CH₂); ¹³C-deptQ-NMR (125 MHz, CDCl₃+1% pyridine-*d*₅): δ = (not all C detected) 155.8 (d, 2C, py-C), 149.8 (d, 2C, α-C), 149.2 (d, 2C, α-C), 140.9 (u, 2C, *o*-C), 138.6 (u, 1C, *p*-C), 134.4 (d, 2C, *m*-C), 132.1 (u, 2C, β-C), 131.8 (u, 2C, β-C), 130.9 (u, 2C, β-C), 130.9 (u, 2C, β-C), 129.1 (u, 2C, py-C), 120.9 (d, 1C, *meso*-C), 107.5 (d, 1C, *meso*-C), 105.3 (u, 2C, *meso*-C), 69.4 (d, 2C, OCH₂), 33.5 (d, 6C, CH₂), 31.8 (d, 2C, CH₂), 31.6 (d, 6C, CH₂), 29.4 (d, 2C, CH₂), 29.4 (d, 2C, CH₂), 29.2 (d, 2C, CH₂), 29.1 (d, 2C, CH₂), 29.0 (d, 2C, CH₂), 28.6 (d, 2C, CH₂), 28.5 (d, 2C, CH₂), 25.0 (d, 2C, CH₂), 24.0 (d, 6C, CH₂), 22.6 (d, 6C, CH₂), 14.1 (u, 6C, CH₃), 14.1 (u, 2C, CH₃), 12.7 (d, 6C, CH₂); *m/z* (MALDI-TOF): 1460.39 (C₉₁H₁₄₃N₅O₂Si₂Zn requires 1461.02).

[5,15-Dibromo-10-(3,5-bis(dodecyloxy)-4-pyridyl)-20-(3,5-bis(trihexylsilyl)-phenyl)-porphyrinato]-zinc(II) (3)

A solution of *N*-bromosuccinimide (NBS) (0.69 g, 3.89 mmol) in chloroform (180 mL) was added dropwise over 10 min to a stirred solution of zinc porphyrin **2** (2.84 g, 1.94 mmol) in pyridine (1.25 mL) and chloroform (70.0 mL). The reaction mixture was stirred at room temperature for 15 min before adding acetone (2 mL) to quench any excess NBS. The solution was concentrated and passed through a short silica plug, eluting with DCM/pyridine (99:1). The solvent was removed from the green filtrate. The green residue was dissolved in chloroform and precipitated by layering methanol. The precipitate was washed with methanol and dried in high vacuum, affording the desired porphyrin **3** (2.80 g, 89%) in the form of purple highly viscous oil.

¹H-NMR (500 MHz, CDCl₃+1% pyridine-*d*₅): δ = 9.58 (d, ³J_{HH} = 4.6 Hz, 2H, β-H), 9.55 (d, ³J_{HH} = 4.6 Hz, 2H, β-H), 8.81 (d, ³J_{HH} = 4.6 Hz, 2H, β-H), 8.70 (d, ³J_{HH} = 4.7 Hz, 2H, β-H), 8.36 (s, 2H, py-H), 8.18 (s, 2H, *o*-H), 7.95 (s, *p*-H), 3.88 (t, ³J_{HH} = 6.3 Hz, 4H, OCH₂), 1.49- 1.41 (m, 12H, CH₂), 1.37-0.76 (m, 96H, CH₂ and CH₃), 0.72-0.64 (m, 4H, CH₂), 0.53-0.44 (m, 8H, CH₂), 0.39-0.29 (m, 4H, CH₂); ¹³C-deptQ-NMR (125 MHz, CDCl₃+1% pyridine-*d*₅): δ = 155.5 (d, 2C, py-C), 150.6 (d, 2C, α-C), 150.4 (d, 2C, α-C), 149.9 (d, 4C, α-C), 140.8 (d, 1C, *ipso*-C), 140.6 (u, 2C, *o*-C), 139.0 (u, 1C, *p*-C), 134.6 (d, 2C, *m*-C), 133.3 (u, 2C, β-C), 133.2 (u, 2C, β-C), 132.4 (u, 2C, β-C), 132.0 (u, 2C, β-C), 128.7 (u, 2C, py-C), 128.5 (d, 1C, py-C), 123.7 (d, 1C, *meso*-C), 110.1 (d, 1C, *meso*-C), 104.3 (d, 2C, *meso*-C), 69.3 (d, 2C, OCH₂), 33.5 (d, 6C, CH₂), 31.8 (d, 2C, CH₂), 31.6 (d, 6C, CH₂), 29.4 (d, 2C, CH₂), 29.3 (d, 2C, CH₂), 29.2 (d, 2C, CH₂), 29.2 (d, 2C, CH₂), 29.0 (d, 2C, CH₂), 28.7 (d, 2C, CH₂), 28.6 (d, 2C, CH₂), 25.1 (d, 2C, CH₂), 24.0 (d, 6C, CH₂), 22.6 (d, 6C, CH₂), 22.6 (d, 2C, CH₂), 14.1 (u, 6C, CH₃), 14.1 (u, 2C, CH₃), 12.6 (d, 6C, CH₂).

[5-(3,5-Bis(dodecyloxy)-4-pyridyl)-15-(3,5-bis(trihexylsilyl)-phenyl)-10,20-(trihexylsilylethynyl)-porphyrinato]-zinc(II) (4)

Dibromoporphyrin **3** (2.80 g, 1.73 mmol, 1.0 equiv.), Pd₂(dba)₃ (155.7 mg, 0.17 mmol, 10 mol%), PPh₃ (136.4 mg, 0.52 mmol, 30 mol%) and CuI (99.0 mg, 0.52 mmol, 30 mol%) were placed in a heat-dried 2-neck 500 mL round-bottom-flask equipped with a tap and a stir bar. The second opening was sealed with a subseal and the flask was evacuated and backfilled with nitrogen three times. In a

heat-dried 2-neck round-bottom-flask with nitrogen inlet and septum, dry toluene (150 mL), dry diisopropylamine (180 mL) and THS-acetylene (1.35 mL, 5.19 mmol, 3.0 equiv.) were freeze-pump-thaw degassed. The solution was cannulated to the solids. The reaction mixture was heated under nitrogen to 50 °C and kept at this temperature for 2 h then filtered over a plug of silica eluting with DCM/pyridine (99:1). The solvents were removed from the green filtrate under reduced pressure. The residue was subjected to column-chromatography on silica eluting with petrol ether/EtOAc/pyridine (10:0.5:1). Purification afforded the desired product **4** (3.06 g, 85 %).

¹H-NMR (400 MHz, CDCl₃+1% pyridine-*d*₅): δ = 9.59 (d, ³J_{HH} = 4.0 Hz, 2H, β-H), 9.57 (d, ³J_{HH} = 4.0 Hz, 2H, β-H), 8.79 (d, ³J_{HH} = 4.0 Hz, 2H, β-H), 8.56 (d, ³J_{HH} = 4.0 Hz, 2H, β-H), 8.47 (s, 2H, py-H), 8.21 (s, 2H, *o*-H), 7.96 (s, 1H, *p*-H), 3.90 (t, ³J_{HH} = 6.4 Hz, 4H, OCH₂), 1.77–1.69 (m, 12H, alkyl-CH₂), 1.55–1.44 (m, 24H, alkyl-CH₂), 1.41–0.76 (m, 48H, alkyl-CH₂), 0.70–0.63 (m, 6H, alkyl-CH₃), 0.50–0.40 (m, 12H, alkyl-CH₃); ¹³C-deptQ-NMR (125 MHz, CDCl₃+1% pyridine-*d*₅): δ = 155.7 (d, 2C, py-C), 152.3 (d, 2C, α-C), 152.1 (d, 2C, α-C), 150.0 (d, 2C, α-C), 149.7 (d, 2C, α-C), 141.0 (d, 1C, *ipso*-C), 140.4 (u, 2C, *o*-C), 139.0 (u, 1C, *p*-C), 134.5 (d, 2C, *m*-C), 132.4 (u, 2C, β-C), 131.5 (u, 2C, β-C), 131.1 (u, 2C, β-C), 130.6 (u, 2C, β-C), 129.0 (u, 2C, py-C), 128.9 (d, 1C, py-C), 124.0 (d, 1C, *meso*-C), 110.7 (d, 1C, *meso*-C), 109.5 (d, 2C, alkynyl-C), 100.6 (d, 2C, *meso*-C), 98.7 (d, 2C, alkynyl-C), 69.6 (d, 2C, OCH₂), 33.5 (d, 6C, CH₂), 33.4 (d, 6C, CH₂), 31.8 (d, 2C, CH₂), 31.7 (d, 6C, CH₂), 31.6 (d, 6C, CH₂), 29.4 (d, 2C, CH₂), 29.2 (d, 2C, CH₂), 29.2 (d, 2C, CH₂), 29.1 (d, 2C, CH₂), 28.9 (d, 2C, CH₂), 28.7 (d, 2C, CH₂), 28.6 (d, 2C, CH₂), 25.1 (d, 2C, CH₂), 24.4 (d, 6C, CH₂), 24.0 (d, 6C, CH₂), 22.7 (d, 6C, CH₂), 22.6 (d, 2C, CH₂), 14.2 (u, 6C, CH₃), 14.2 (u, 6C, CH₃), 14.1 (u, 2C, CH₃), 13.9 (d, 6C, CH₂-Si), 12.7 (d, 6C, CH₂-Si); *m/z* (MALDI-TOF): 2071.90 (C₁₃₁H₂₁₉N₅O₂Si₄Zn requires 2070.56).

[5-(3,5-Bis(dodecyloxy)-4-pyridyl)-10-ethynyl-15-(3,5-bis(trihexylsilyl)-phenyl)-20-(trihexylsilylethynyl)-porphyrinato]-zinc(II) (**5**)

Porphyrin monomer **4** (3.0 g, 1.48 mmol, 1.0 equiv.) was dissolved in dry DCM (40 mL) and CHCl₃ (40 mL). Pyridine (4.0 mL) was added. Under stirring TBAF solution (1.0 M in THF; 1.03 mL, 1.03 mmol, 0.7 equiv.) was added dropwise. The reaction was monitored by TLC. After 20 min a good product ratio was reached. The mixture was filtered over a plug of silica eluting with DCM/pyridine (50:1). The solvent was removed from the green filtrate and the residue was subjected to column-chromatography on silica eluting with petrol ether/EtOAc/pyridine 20:2:1. Recovered starting material porphyrin monomer **4** (1.74 g, 57%), desired product **5** (893 mg, 34%), and fully deprotected material (156.2 mg, 27%) were isolated in form of their pyridyl-complexes as dark purple semi-solids.

¹H-NMR (400 MHz, CDCl₃+1% pyridine-*d*₅): δ = 9.59 (m, 4H, β-H), 8.82 (t, ³J_{HH} = 4.0 Hz, 2H, β-H), 8.71 (t, ³J_{HH} = 4.4 Hz, 2H, β-H), 8.45 (s, 2H, py-H), 8.21 (s, 2H, *o*-H), 7.95 (s, 1H, *p*-H), 4.06 (s, 1H, ethynyl-H), 3.90 (t, ³J_{HH} = 6.4 Hz, 4H, OCH₂), 1.77–1.69 (m, 6H, alkyl-CH₂), 1.53–0.37 (m, 83H, alkyl-CH₃); *m/z* (MALDI-TOF): 1790.29 (C₁₁₃H₁₈₁N₅O₂Si₃Zn requires 1788.28).

Dimerization of [5-(3,5-bis(dodecyloxy)-4-pyridyl)-10-ethynyl-15-(3,5-bis(trihexylsilyl)-phenyl)-20-(trihexylsilylethynyl)-porphyrinato]-zinc(II) (synthesis of dimer (**6**), **P2py2-Zn**)

Pd(PPh₃)₂Cl₂ (28.1 mg, 0.04 mmol, 8.0 mol%), copper(I) iodide (45.0 mg, 0.32 mmol, 0.65 equiv.) and 1,4-benzoquinone (102.7 mg, 0.95 mmol, 1.90 equiv.) were dissolved in dry toluene (50 mL) and dry DIPA (15 mL) at 20 °C. The yellow solution was added to monodeprotected-porphyrin **5** (893.0 mg, 0.5 mmol, 1.0 equiv.). The reaction mixture was stirred at 20 °C for 2 h then filtered over a plug of silica eluting with DCM/pyridine (99:1). Solvents were removed from the filtrate under reduced pressure and then the residue was purified by SEC-column chromatography, affording the desired dimer **6** in 95% yield (848.2 mg).

$^1\text{H-NMR}$ (400 MHz, $\text{CDCl}_3+1\%$ pyridine- d_5): δ = 9.81 (d, J = 4.5 Hz, 2H, β -H), 9.78 (d, J = 4.5 Hz, 2H, β -H), 9.61 (d, J = 4.5 Hz, 2H, β -H), 9.58 (d, J = 4.5 Hz, 2H, β -H), 8.90 (d, J = 4.5 Hz, 2H, β -H), 8.81 (d, J = 4.5 Hz, 2H, β -H), 8.79 (d, J = 4.5 Hz, 2H, β -H), 8.71 (d, J = 4.5 Hz, 2H, β -H), 8.49 (s, 4H, py-H), 8.25 (s, 4H, *o*-H), 7.98 (s, 2H, *p*-H), 3.95 (t, J = 6.3 Hz, 8H, OCH_2), 1.77–1.69 (m, 12H, alkyl-H), 1.55–1.24 (m, 150H, alkyl-H), 1.00–0.45 (m, 230H, alkyl-H).; $^{13}\text{C-deptQ-NMR}$ (125 MHz, $\text{CDCl}_3+1\%$ pyridine- d_5): δ = 155.7 (d, 4C, py-C), 153.1 (d, 2C, α -C), 152.8 (d, 2C, α -C), 152.3 (d, 2C, α -C), 152.1 (d, 2C, α -C), 150.3 (d, 2C, α -C), 150.0 (d, 2C, α -C), 149.9 (d, 2C, α -C), 149.7 (d, 2C, α -C), 140.9 (d, 2C, *ipso*-C), 140.6 (u, 4C, *o*-C), 139.1 (u, 2C, *p*-C), 134.7 (d, 4C, *m*-C), 132.9 (u, 2C, β -C), 132.5 (u, 2C, β -C), 131.7 (u, 2C, β -C), 131.6 (u, 2C, β -C), 131.3 (u, 2C, β -C), 131.2 (u, 2C, β -C), 130.8 (u, 2C, β -C), 130.4 (u, 2C, β -C), 129.0 (u, 4C, py-C), 128.7 (d, 2C, py-C), 124.7 (d, 2C, *meso*-C), 111.4 (d, 2C, *meso*-C), 109.5 (d, 2C, alkynyl-C), 101.4 (d, 2C, *meso*-C), 99.3 (d, 4C, *meso*-C and alkynyl-C), 88.1 (d, 2C, alkynyl-C), 82.1 (d, 2C, alkynyl-C), 69.7 (d, 4C, OCH_2), 33.6 (d, 12C, CH_2), 33.4 (d, 6C, CH_2), 31.8 (d, 4C, CH_2), 31.7 (d, 6C, CH_2), 31.7 (d, 12C, CH_2), 29.5 (d, 4C, CH_2), 29.3 (d, 4C, CH_2), 29.2 (d, 4C, CH_2), 29.1 (d, 4C, CH_2), 28.8 (d, 4C, CH_2), 28.7 (d, 4C, CH_2), 25.2 (d, 4C, CH_2), 24.4 (d, 6C, CH_2), 24.1 (d, 12C, CH_2), 22.8 (d, 6C, CH_2), 22.7 (d, 12C, CH_2), 22.6 (d, 4C, CH_2), 14.2 (u, 18C, CH_3), 14.1 (u, 4C, CH_3), 13.9 (d, 6C, CH_2 -Si), 12.7 (d, 12C, CH_2 -Si); m/z (MALDI-TOF): 3583.14 ($\text{C}_{226}\text{H}_{360}\text{N}_{10}\text{O}_4\text{Si}_6\text{Zn}_2$ requires 3580.55)

Demetallation of zinc dimer **P2py2-Zn (6)** (synthesis of free-base dimer (7), **P2py2**)

Zinc porphyrin dimer (**6**) (159.5 mg, 0.045 mmol, 1.0 equiv.) was dissolved in chloroform (50 mL). TFA (0.69 mL, 9.0 mmol, 200 equiv.) was added dropwise under stirring. After 10 min pyridine (6.0 mL) was added and the green mixture was directly filtered over a plug of silica eluting with chloroform. Solvents were removed from the filtrate under reduced pressure affording free-base dimer **7**, **P2py2** in 95% yield (145.3 mg).

$^1\text{H-NMR}$ (400 MHz, CDCl_3): δ = 9.80 (t, J = 4.6 Hz, 4H, β -H), 9.59 (t, J = 4.6 Hz, 4H, β -H), 8.89 (d, J = 4.4 Hz, 2H, β -H), 8.81 (t, J = 3.4 Hz, 4H, β -H), 8.71 (d, J = 4.6 Hz, 2H, β -H), 8.53 (s, 4H, py-H), 8.28 (s, 4H, *o*-H), 8.02 (s, 2H, *p*-H), 4.02 (t, J = 6.3 Hz, 8H, OCH_2), 1.77–1.69 (m, 12H, alkyl-H), 1.57–1.26 (m, 150H, alkyl-H), 1.07–0.47 (m, 240H, alkyl-H), -1.82 (s, 4H, NH). $^{13}\text{C-deptQ-NMR}$ (125 MHz, CDCl_3): δ = 155.6 (d, 4C, py-C), 140.6 (u, 4C, *o*-C), 139.7 (u, 2C, *p*-C), 135.4 (d, 4C, *m*-C), 129.1 (u, 4C, py-C), 127.0 (d, 2C, py-C), 124.2 (d, 2C, *meso*-C), 111.3 (d, 2C, *meso*-C), 107.9 (d, 2C, alkynyl-C), 101.8 (d, 2C, *meso*-C), 101.5 (d, 2C, *meso*-C), 99.1 (d, 2C, alkynyl-C), 87.3 (d, 2C, alkynyl-C), 82.7 (d, 2C, alkynyl-C), 69.9 (d, 4C, OCH_2), 33.7 (d, 12C, CH_2), 33.5 (d, 6C, CH_2), 31.8 (d, 4C, CH_2), 31.8 (d, 6C, CH_2), 31.8 (d, 12C, CH_2), 29.4 (d, 4C, CH_2), 29.3 (d, 4C, CH_2), 29.2 (d, 4C, CH_2), 29.1 (d, 4C, CH_2), 29.0 (d, 4C, CH_2), 28.8 (d, 4C, CH_2), 28.7 (d, 4C, CH_2), 25.3 (d, 4C, CH_2), 24.5 (d, 6C, CH_2), 24.2 (d, 12C, CH_2), 22.8 (d, 6C, CH_2), 22.8 (d, 12C, CH_2), 22.7 (d, 4C, CH_2), 14.3 (u, 18C, CH_3), 14.1 (u, 4C, CH_3), 13.9 (d, 6C, CH_2 -Si), 12.8 (d, 12C, CH_2 -Si); m/z (MALDI-TOF): 3455.99 ($\text{C}_{226}\text{H}_{364}\text{N}_{10}\text{O}_4\text{Si}_6$ requires 3453.73); UV/Vis: λ_{max} [nm] ($\epsilon/\text{mol}^{-1}\text{Lcm}^{-1}$) (toluene) = 451 (3.35×10^5), 485 (1.47×10^5), 626 (6.45×10^4), 731 (8.77×10^4).

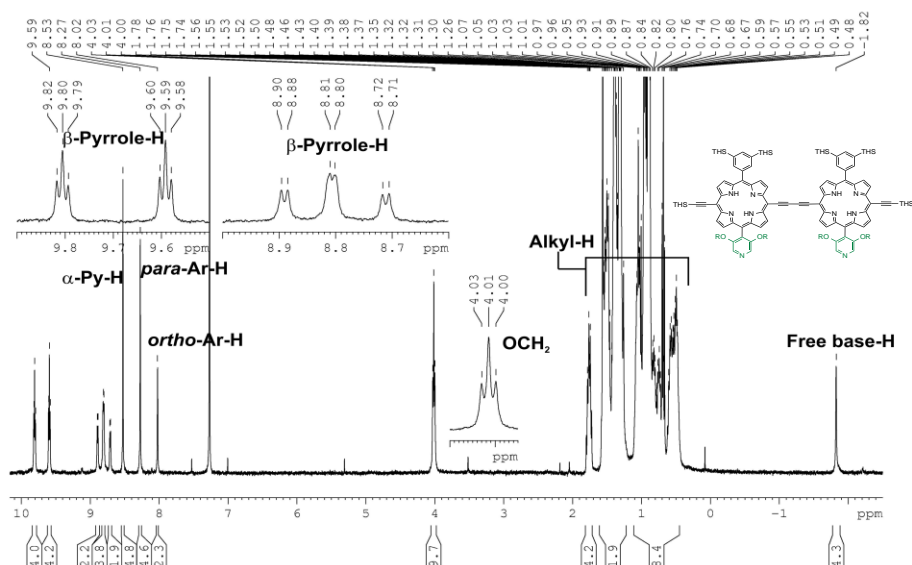


Figure S1 The $^1\text{H-NMR}$ spectrum of **P2Py2** (CDCl_3 , 298 K, 400 MHz)

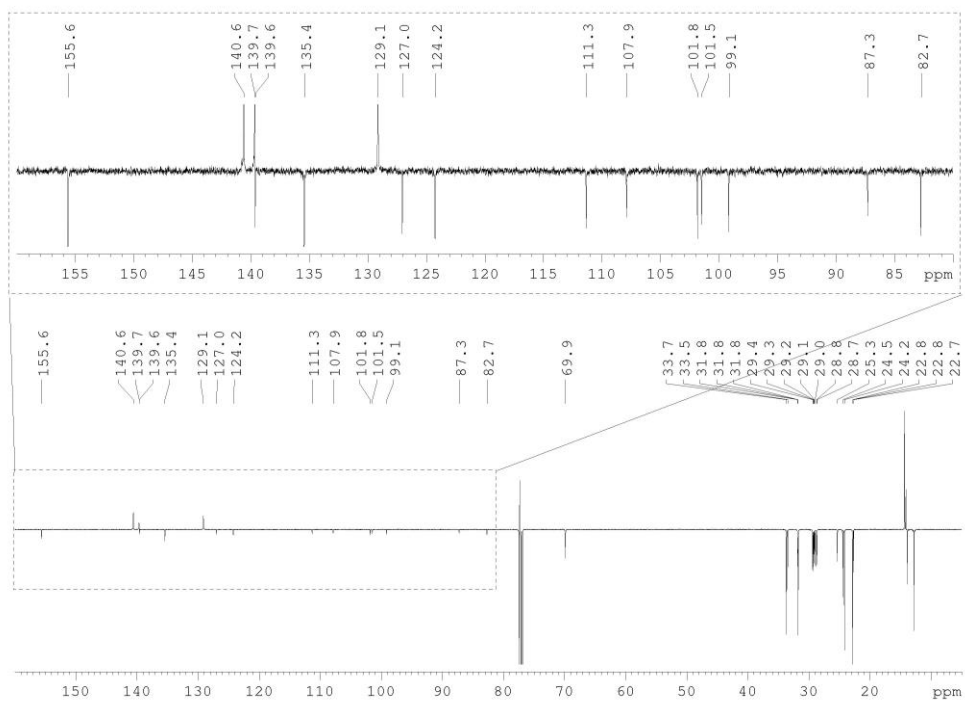


Figure S2 The $^{13}\text{C-DEPT Q-NMR}$ spectrum of **P2Py2** (CDCl_3 , 298 K, 125 MHz)

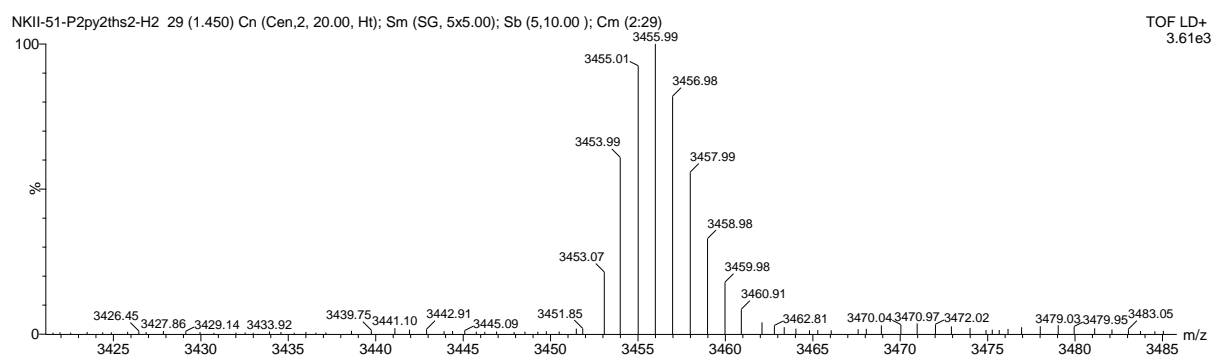
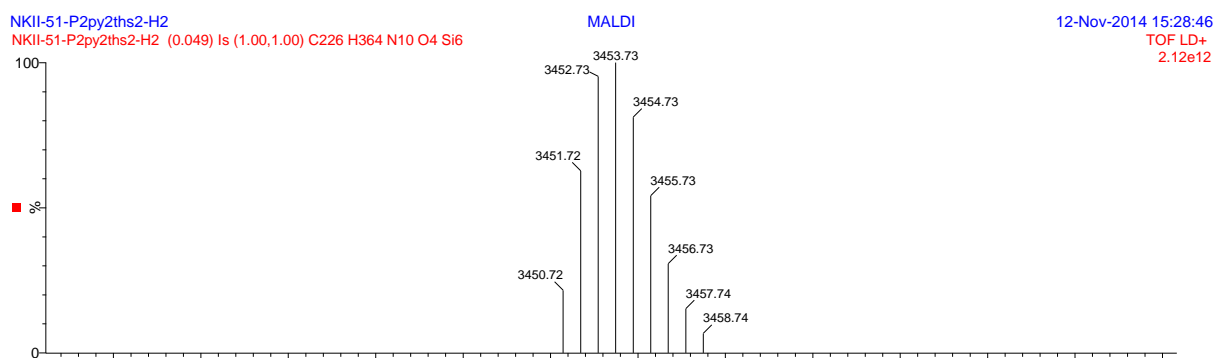
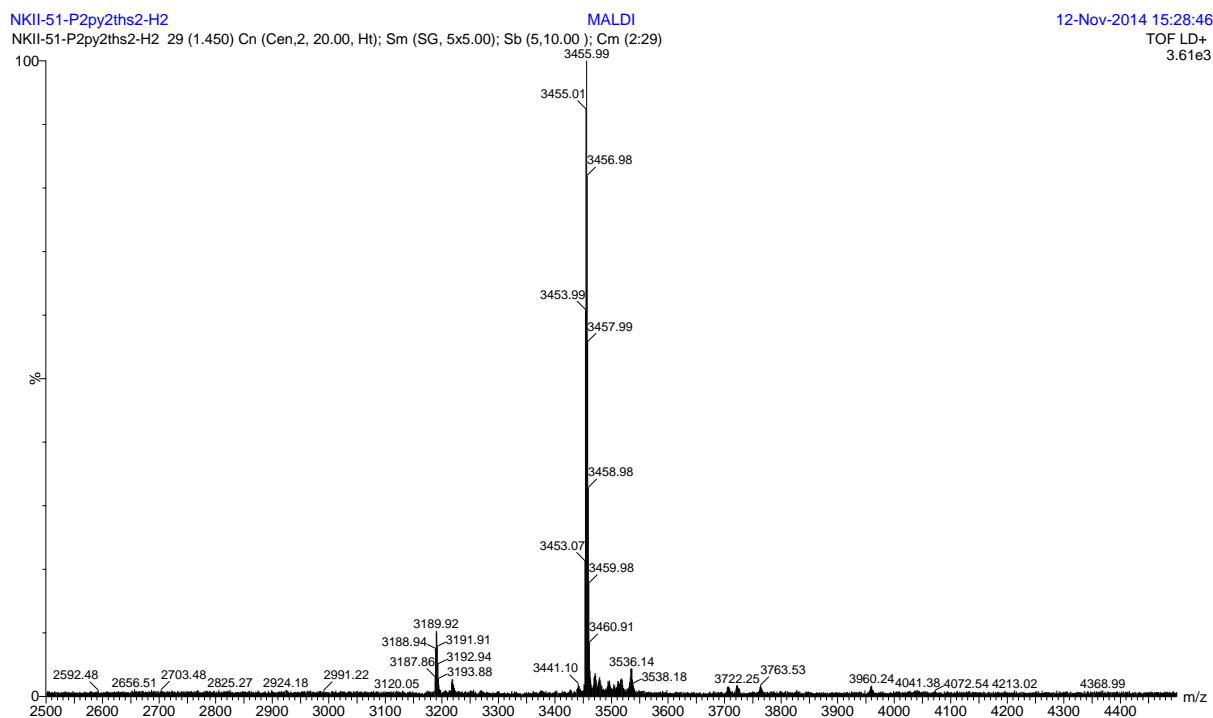


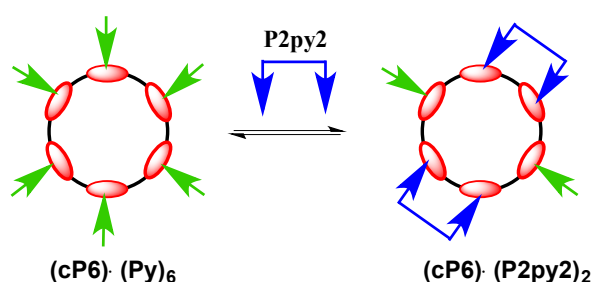
Figure S3 The MALDI-ToF mass spectra of **P2Py2** (DTCB matrix). m/z of **P2Py2** is 3455.99 ($C_{226}H_{364}N_{10}O_4Si_6$ requires 3453.73).

C. Determination of stoichiometries of complexes

Binding stoichiometries of all complexes were evaluated by Job plot analysis by means of UV/Vis/NIR spectroscopy. Total concentrations of all components were kept constant while varying the molar ratios of guest (**P2py2**) to host (**rings**).

C1. ^1H -NMR of $c\text{-P6}\cdot\text{P2py2}$ complex to confirm the stoichiometry

A ^1H NMR titration was performed to test the conclusion of the Job plot on the formation of a 1:2 complex between $c\text{-P6}$ and P2py2 . Upon adding dimer P2Py2 to $c\text{-P6}$, the appearance of a new complex and the shifting of all peaks corresponding to $c\text{-P6}$ were observed (Figure S4). The rate of exchange is intermediate between fast and slow, resulting in broadening of the resonances, so that it was not possible to gain much information directly from the resonances of $c\text{-P6}$ or P2py2 . At the start of the titration, 6.0 equivalents of pyridine were present and bound to the 6-ring. (The amount of pyridine was determined from the ^1H NMR spectrum at 0.0 equivalent of P2py2 using the integration of the pyridine in comparison to the value of the porphyrin $c\text{-P6}$.) The pyridine that was initially bound to $c\text{-P6}$ was replaced by dimer during the titration, because when P2Py2 chelates to $c\text{-P6}$ it binds much more strongly than monodentate pyridine (Scheme S2). Therefore, the shift of the peaks corresponding to the pyridine could be used to monitor the fraction of bound pyridine, and thus to determine how many equivalents of dimer bind to each 6-ring.



Scheme S2 Possible displacement of pyridine (green arrows) with P2py2 during ^1H NMR titration of $c\text{-P6}$ with P2Py2 when pyridine is present.

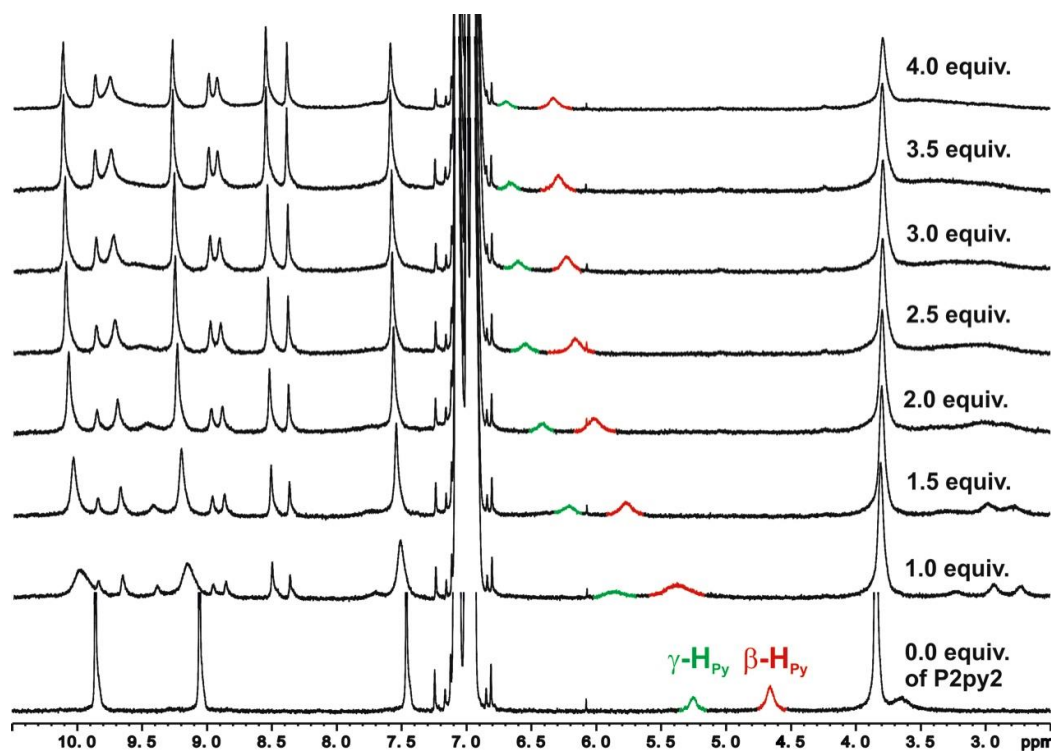


Figure S4 ^1H NMR titration of $c\text{-P6}\cdot(\text{Py})_6$ with P2Py2 (toluene- d_8 , 298 K, 500 MHz, $[c\text{-P6}] = 0.22$ mM) and assignment of ratio of $\text{P2Py2}/c\text{-P6}$. Red and green peaks correspond to β - and γ -protons on pyridine, respectively.

We calculated the chemical shift of the peaks corresponding to the β - and γ -pyridine protons during the titration using the equation:

$$\delta_{obs} = \frac{[\mathbf{Py}]_{free}}{[\mathbf{Py}]_{tot}} \delta_{free} + \frac{[\mathbf{Py}]_{bound}}{[\mathbf{Py}]_{tot}} \delta_{bound} \quad (\text{eq. 3.1})$$

where $[\mathbf{Py}]_{free}$, $[\mathbf{Py}]_{bound}$ and $[\mathbf{Py}]_{tot}$ are concentrations of free, bound and total pyridine in the titration, respectively; δ_{obs} , δ_{free} and δ_{bound} (ppm) are chemical shifts corresponding to β - or γ -protons of observed, free and fully bound pyridine, respectively. The chemical shifts corresponding to free β - and γ -pyridine are $\delta = 6.67$ and 6.99 ppm, respectively (measured by recording the ^1H NMR spectrum of pyridine in toluene- d_8).

As there is no consumption of components, it is true that

$$[\mathbf{Py}]_{tot} = [\mathbf{Py}]_{bound} + [\mathbf{Py}]_{free} \quad (\text{eq. 3.2}).$$

$[\mathbf{Py}]_{bound}$ can be obtained from the binding constant K_{py} , making the following assumptions. Prior to additional of dimer, all 6 sites of Zn on the 6-ring are available for binding pyridine. After additional of up to two equivalents of dimer, some of the Zn sites bind dimer to form a 1:2 complex, making them unavailable for binding weak ligands such as pyridine. When more than two equivalents of dimer are added, only two Zn sites are available for binding pyridine; they can bind to either pyridine and/or excess dimer which acts as the competitive ligand. We assume that the dimer can bind to these remaining sites as a non-chelating ligand, so the concentration of these pyridine sites is twice the concentration of excess dimer. Thus, after more than two equivalents of dimer, the effective pyridine concentration is not only obtained from the concentration of simply pyridine but also two times of concentration of excess dimer.

Then, $[\text{eff. Py}]_{bound}$ is given from

$$[\text{eff. Py}]_{bound} = \frac{(K_{py}([\text{eff. Zn}]_{tot} + [\text{eff. Py}]_{tot}) + 1) - \sqrt{(K_{py}([\text{eff. Zn}]_{tot} + [\text{eff. Py}]_{tot}) + 1)^2 - 4K_{py}^2[\text{eff. Zn}]_{tot}[\text{eff. Py}]_{tot}}}{2K_{py}} \quad (\text{eq. 3.3})$$

where K_{py} is the association constant between pyridine and porphyrin monomer ($K_{py} = (2.58 \pm 0.26) \times 10^4 \text{ M}^{-1}$, see detail in the determination of reference constants **Section 3.3.3**); $[\text{eff. Zn}]_{tot}$ is the total concentration of the available Zn sites to weak binding of ligands such as pyridine; $[\text{eff. Py}]_{tot}$ is the total concentration of the effective pyridine sites. $[\text{eff. Zn}]_{tot}$ and $[\text{eff. Py}]_{tot}$ are derived from the 1:2 assumption below:

For $[\text{eff. Zn}]_{tot}$

Condition a) if the amount of dimer is less than or equal to 2 equivalents, then all dimers are bound to the 6-ring, giving:

$$[\mathbf{Zn}]_{tot} = 6[\mathbf{cP6}]_{tot} - 2[\mathbf{P2py2}]_{tot} \quad (\text{eq. 3.4})$$

Condition b) if the amount of dimer is more than 2 equivalents, then there are only 2 sites of zinc available on each 6-ring, giving:

$$[\mathbf{Zn}]_{tot} = 2[\mathbf{cP6}]_{tot} \quad (\text{eq. 3.5})$$

For $[\text{eff. Py}]_{\text{tot}}$

Condition a) if the amount of dimer is less than or equal to 2 equivalents, then all dimers are bound to the 6-ring and the total concentration of effective pyridine is just the total concentration of ordinary pyridine, $[\text{Py}]_{\text{tot}}$, giving

$$[\text{eff. Py}]_{\text{tot}} = [\text{Py}]_{\text{tot}} \quad (\text{eq. 3.6})$$

$$\text{and } [\text{Py}]_{\text{bound}} = [\text{eff. Py}]_{\text{bound}} \quad (\text{eq. 3.7}).$$

Condition b) if the amount of dimer is more than 2 equivalents, then the excess dimer can also compete with the pyridine to bind to the zinc site. If we consider the dimer as two sites of pyridine, we obtain

$$[\text{eff. Py}]_{\text{tot}} = [\text{Py}]_{\text{tot}} + 2[\text{non-chelating dimer}]_{\text{tot}} \quad (\text{eq. 3.8}).$$

Since we assume that two dimers can be bound on the 6-ring, it is true that

$$[\text{non-chelating dimer}]_{\text{tot}} = [\text{P2py2}]_{\text{tot}} - 2[\text{cP6}]_{\text{tot}} \quad (\text{eq. 3.9}).$$

Then,

$$[\text{eff. Py}]_{\text{tot}} = [\text{Py}]_{\text{tot}} + 2[\text{P2py2}]_{\text{tot}} - 4[\text{cP6}]_{\text{tot}} \quad (\text{eq. 3.10})$$

$$\text{and } [\text{Py}]_{\text{bound}} = [\text{eff. Py}]_{\text{bound}} \times \left(\frac{[\text{Py}]_{\text{tot}}}{[\text{Py}]_{\text{tot}} + 2[\text{P2py2}]_{\text{tot}} - 4[\text{cP6}]_{\text{tot}}} \right) \quad (\text{eq. 3.11}).$$

This equation was combined with **Equations 3.5** and **3.3** to calculate the chemical shifts of the pyridine signals over the course of the titration as shown in Figure S5. The predicted chemical shifts of pyridine are in very good agreement with the empirical data from the titration, indicating that the 1:2 assumption is valid and only two dimers are bound to 6-ring. This 1:2 ratio can be explained by the increased strain in the ring upon binding **P2py2** to **c-P6**, which may straighten out the binding sites on **c-P6**. This may disfavour the formation of the 1:3 (**c-P6:P2py2**) complex.

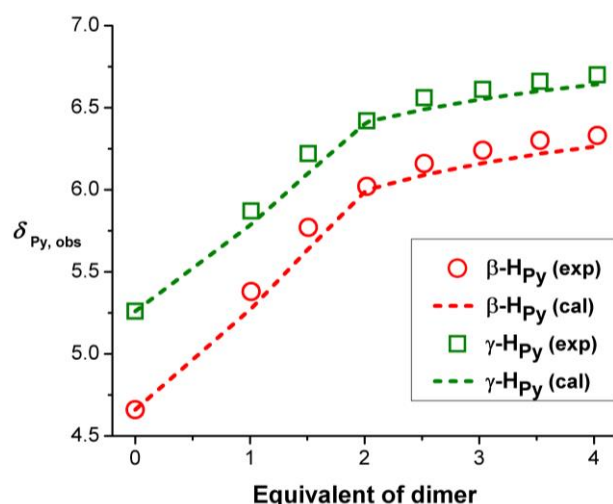


Figure S5 Changes in the chemical shift of the pyridine protons on titration of **c-P6•(py)₆** with **P2py2**, showing the γ -proton (green square) and β -proton (red circle) with various equivalent of dimer **P2py2**. The simulated data were calculated by equation 3.3 (green dash line, γ -proton and red dash line, β -proton).

D. Determination of binding constant, K_f

All titrations were repeated at least twice to check reproducibility. All titrations were carried out in toluene at 25 °C.

D1. UV/Vis formation titration

At the first attempt to determine the binding constant (K_f) in toluene at 25 °C, UV/Vis/NIR formation titrations of $(\mathbf{c-PN}) \cdot (\mathbf{P2py2})_{N/2}$ complexes were performed. The dimer was added to the nanoring and the concentration of the nanorings was kept constant during the titration to inspect the isosbesticity and to simplify the analysis of the data. Binding constants were determined from the titration curves using a 1:1 binding model (i.e. the dimer ligands behave independently in their binding to N -ring, and N -ring is treated as $N/2$ dimer sites). Isosbestic behavior would be observed if this assumption were fulfilled in the actual system. The binding isotherm was analyzed by fitting in Origin[®] software, assuming a 1:1 binding situation. K_f was evaluated by

$$\frac{A-A_0}{A_f-A_0} = \frac{(K_f([L]_0+[P]_0)+1) - \sqrt{(K_f([L]_0+[P]_0)+1)^2 - 4K_f^2[P]_0[L]_0}}{2K_f[P]_0}, \quad (\text{eq. 12})$$

where A is the observed absorption at a specific wavelength or difference of absorption at two wavelengths; A_0 is the starting absorption at this wavelength or difference of absorption in these two wavelengths; A_f is the asymptotic final absorption at this wavelength or difference of absorption in these two wavelengths; K_f is the association constant between ligand and porphyrin host; $[L]$ is the concentration of ligand; $[P]_0$ is the concentration of porphyrin host.

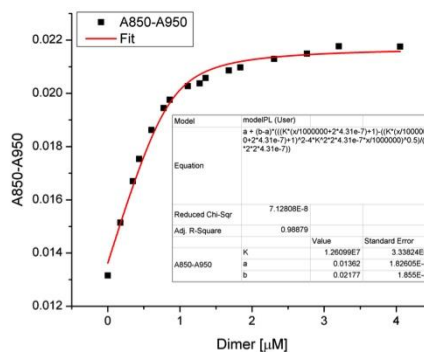
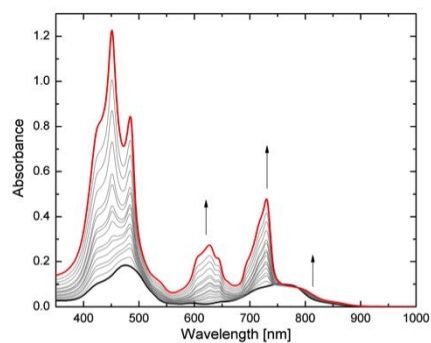
For the formation titration of $\mathbf{c-P10}$ and $\mathbf{c-P12}$ -dimer complexes, we encountered aggregation problems between the nanorings at the initial points of the titration, so these initial points were excluded from the analysis.

The UV/Vis/NIR formation titration spectra are shown in Figures S6–S9. The binding constants of the complexes are mostly too strong ($K_f > 10^7 \text{ M}^{-1}$ as listed in Table 1) to be determined from formation titrations. Thus, denaturation titrations were used to determine K_f indirectly via the denaturation constant K_{dn} .

Table S1 Binding constants of $\mathbf{c-PN}$ with $\mathbf{P2py2}$ (1:1 association constant, M^{-1}) determined by direct titration

$\mathbf{c-PN}$	K_f, M^{-1}		
	Run 1	Run 2	Average
$\mathbf{c-P6}$	$(1.26 \pm 0.33) \times 10^7$	$(1.05 \pm 0.15) \times 10^7$	$(1.16 \pm 0.18) \times 10^7$
$\mathbf{c-P8}$	$(2.88 \pm 0.41) \times 10^7$	$(3.07 \pm 0.47) \times 10^7$	$(2.98 \pm 0.31) \times 10^7$
$\mathbf{c-P10}$	$(1.70 \pm 0.19) \times 10^7$	$(1.43 \pm 0.18) \times 10^7$	$(1.57 \pm 0.13) \times 10^7$
$\mathbf{c-P12}$	$(2.79 \pm 0.59) \times 10^7$	$(2.71 \pm 0.47) \times 10^7$	$(2.75 \pm 0.37) \times 10^7$

Run 1:



Run 2:

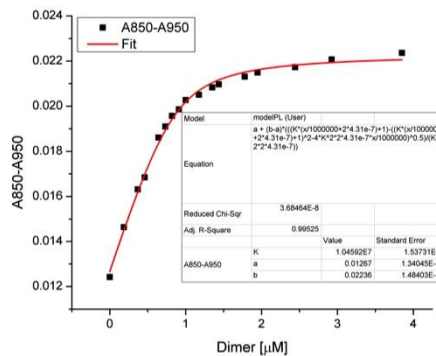
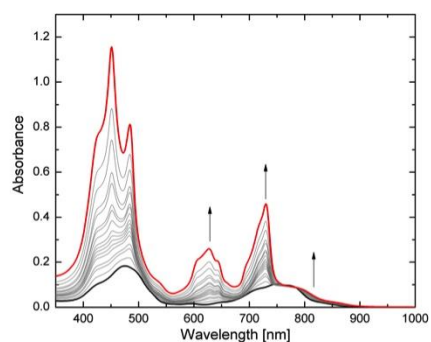
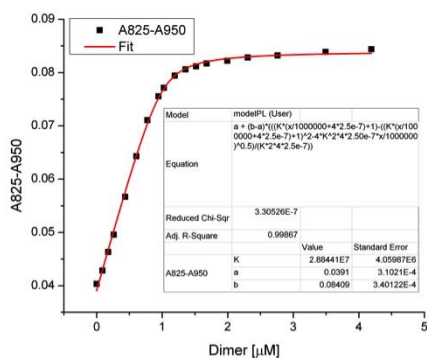
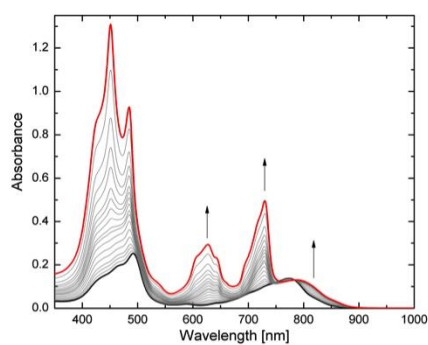


Figure S4 UV/Vis/NIR formation titration of *c*-P6 ($[c\text{-P6}] = 4.31 \times 10^{-7} \text{ M}$) with P2py2 in toluene at 298 K (Run 1: $R^2 = 0.989$; Run 2: $R^2 = 0.995$). (left) Changes in absorption upon addition of P2py2. Arrows indicate areas of increasing and decreasing absorption during the titration; (right) Binding isotherm (black dots) derived from absorption data at $\lambda = 850 - 950 \text{ nm}$ and fit obtained from Origin[®] (red line).

Run 1:



Run 2:

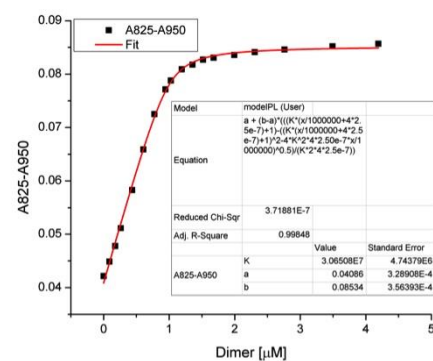
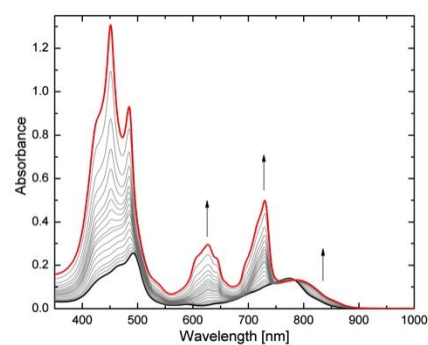
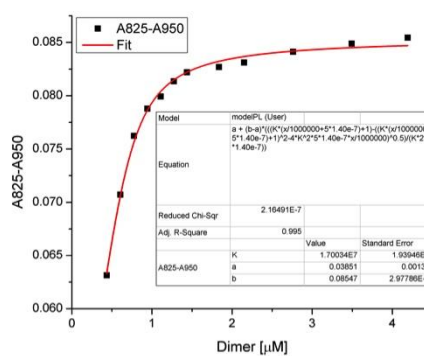
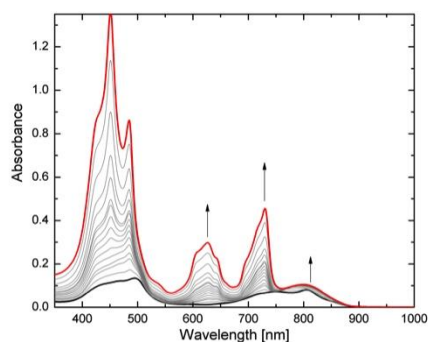


Figure S5 UV/Vis/NIR formation titration of **c-P8** [$c-P8$] = 2.50×10^{-7} M) with **P2py2** in toluene at 298 K (Run 1: $R^2 = 0.999$; Run 2: $R^2 = 0.998$). (left) Changes in absorption upon addition of P2py2. Arrows indicate areas of increasing and decreasing absorption during the titration; (right) Binding isotherm (black dots) derived from absorption data at $\lambda = 825 - 950$ nm and fit obtained from Origin® (red line).

Run 1:



Run 2:

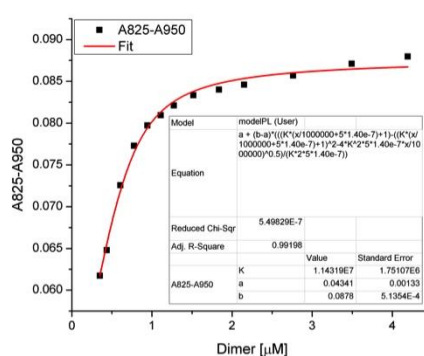
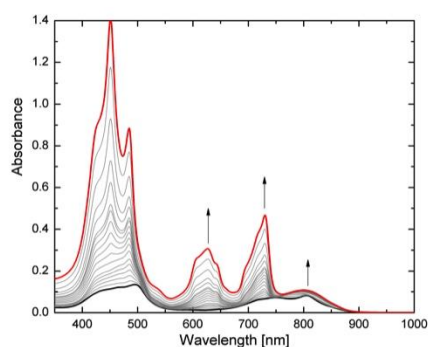
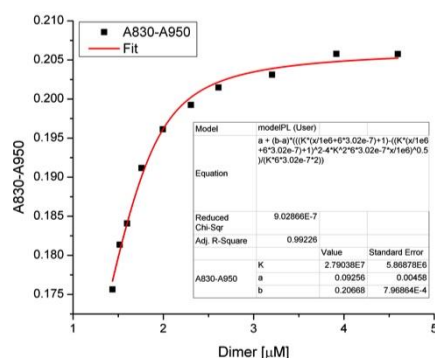
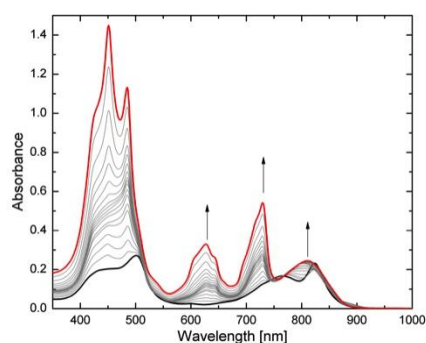


Figure S6 UV/Vis/NIR formation titration of *c*-P10 ($[c\text{-P10}] = 1.40 \times 10^{-7} \text{ M}$) with P2py2 in toluene at 298 K (Run 1: $R^2 = 0.995$; Run 2: $R^2 = 0.992$). (left) Changes in absorption upon addition of P2py2. Arrows indicate areas of increasing and decreasing absorption during the titration; (right) Binding isotherm (black dots) derived from absorption data at $\lambda = 825 - 950 \text{ nm}$ and fit obtained from Origin® (red line).

Run 1:



Run 2:

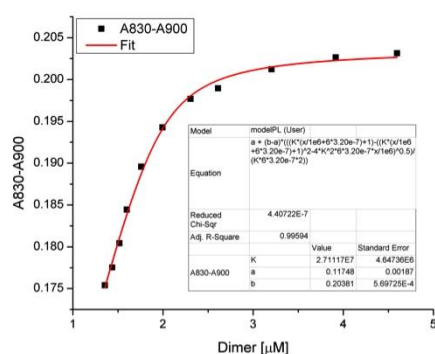
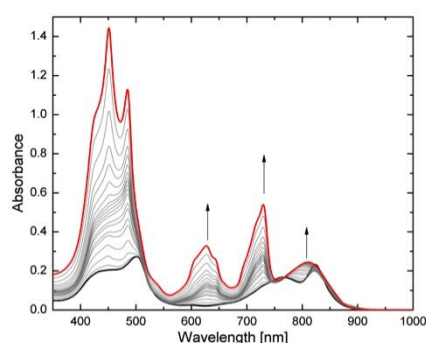


Figure S7 UV/Vis/NIR formation titration of with **c-P12** ($[c-P12] = 3.02 \times 10^{-7} M$) with **P2py2** in toluene at 298 K (Run 1: $R^2 = 0.992$; Run2: $R^2 = 0.996$). (left) Changes in absorption upon addition of **P2py2**. Arrows indicate areas of increasing and decreasing absorption during the titration; (right) binding isotherm (black dots) derived from absorption data at $\lambda = 830 - 950$ nm and fit obtained from Origin® (red line).

D2. UV/Vis denaturation titration

The self-assembled complexes were generated by titrating solutions of **c-PN** ($N = 6, 8, 10$ and 12) in toluene with pyridyl substituted-porphyrin dimer **P2py2**. UV/Vis/NIR denaturation titrations were used to determine K_f indirectly via the denaturation constant K_{dn} . At approximately $10^{-6} M$ in toluene at 25 °C, a large excess of pyridine was titrated to the complexes of $(c-PN) \bullet (P2py2)_{N/2}$ (except for **c-P6**, which is a $(c-P6) \bullet (P2py2)_2$ complex) to displace bidentate ligand **P2py2**. The denaturation data were analyzed by fitting in Origin® software, assuming a 1:1 binding situation. K_{dn} was evaluated by

$$K_{dn} = \frac{[c-PN \cdot Py_2][P2py_2]}{[c-PN \cdot P2py_2][Py]^2}, \quad (\text{eq. 13})$$

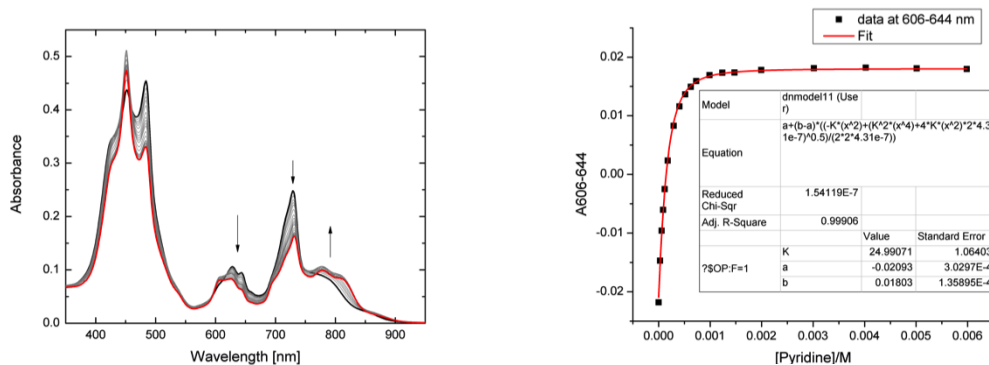
where $[Py]$ is the concentration of pyridine. The corresponding binding isotherm was given by

$$\frac{A - A_0}{A_f - A_0} = \frac{-K_{dn}[Py]^2 + \sqrt{K_{dn}^2[Py]^4 + 4K_{dn}[Py]^2[P]_0}}{2[P]_0}, \quad (\text{eq. 14})$$

where A is the observed absorption at a specific wavelength or difference of absorption at two wavelengths; A_0 is the starting absorption at this wavelength or difference of absorption in these

two wavelengths; A_f is the asymptotic final absorption at this wavelength or difference of absorption in these two wavelengths; K_{dn} is the denaturation constant between **P2py2** and the porphyrin nanoring complex; [Py] is the concentration of pyridine and $[P]_0$ is the concentration of porphyrin nanoring complex. Since we are using a 1:1 binding model, the $[P]_0$ is a 2, 4, 5 or 6-fold multiple of the concentration of **c-P6**, **c-P8**, **c-P10** and **c-P12**, respectively as they have multiple porphyrin units inside each molecule. The UV/Vis denaturation titrations are shown in Figures S10-S13. Binding isotherms were derived from the changes in absorption at two specific wavelengths. Wavelengths were chosen which gave the greatest increase and decrease in absorption during each titration, within the same region of the spectrum. We use a difference in absorption, resulting from complexation, to avoid any effects that might cause variation in the baseline, since such artefacts would cause a rise or fall in the absorption at both wavelengths. Binding isotherms derived from the changes in absorption at selected wavelengths were analyzed by simulation with equation 12 to give the smooth curves plotted in Figures S10-S13 (right), with just three free parameters (A_0 , A_f , and K_{dn}). The resulting values of K_{dn} are listed in Table S2 in Section D4.

Run 1:



Run 2:

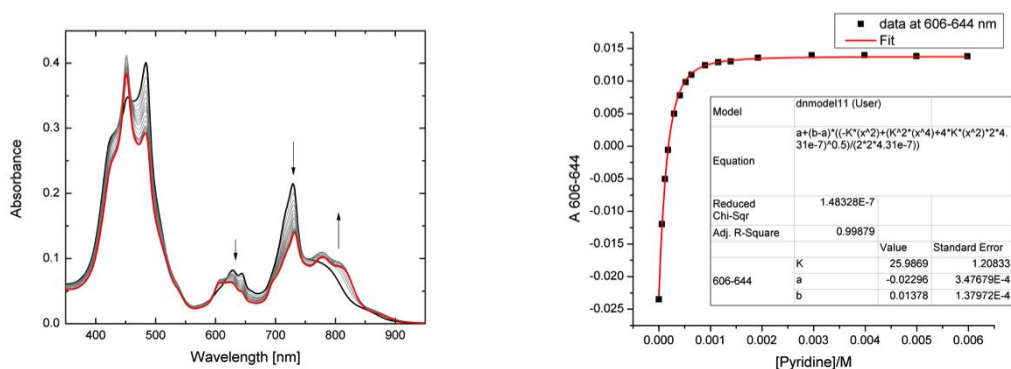
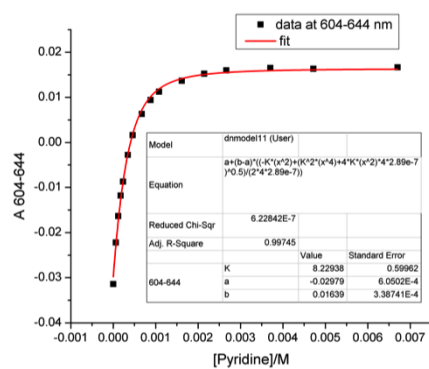
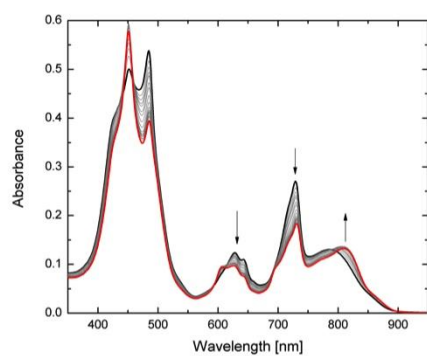


Figure S8 UV/Vis/NIR denaturation titration of **(c-P6)₂(P2py2)₂** ($[complex] = 4.31 \times 10^{-6} M$) with pyridine in toluene at 298 K (Run1: $R^2 = 0.999$; Run2: $R^2 = 0.999$). (left) Changes in absorption upon addition of pyridine. Arrows indicate areas of increasing and decreasing absorption during the titration; (right) Binding isotherm (black dots) derived from absorption data at $\lambda = 606 - 644$ nm and fit obtained from Origin[®] (red line).

Run 1:



Run 2:

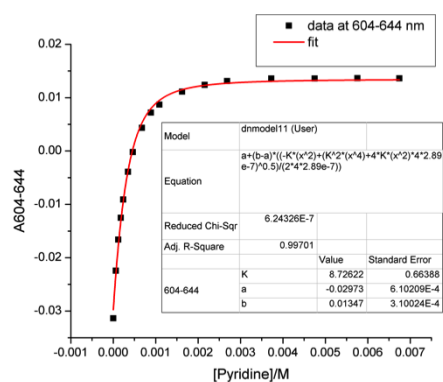
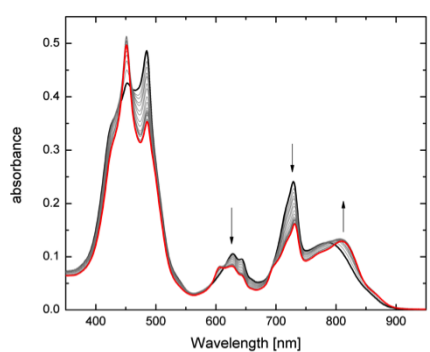
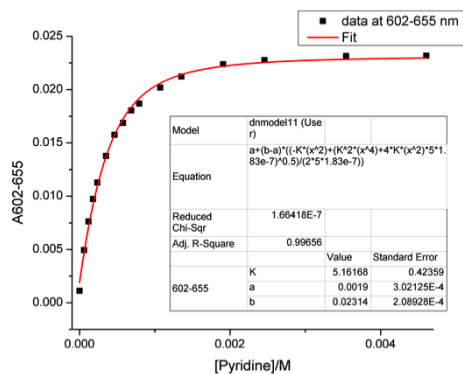
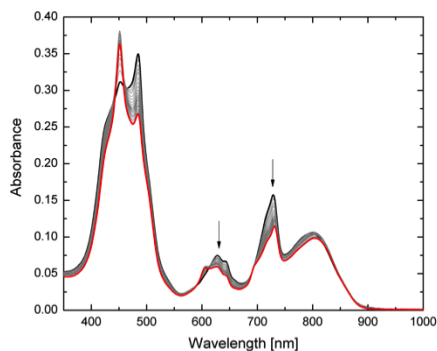


Figure S9 UV/Vis/NIR denaturation titration of $(c-P8) \bullet (P2py2)_4$ ($[complex] = 2.89 \times 10^{-7} M$) with pyridine in toluene at 298 K (Run 1: $R^2 = 0.997$; Run 2: $R^2 = 0.997$). (left) Changes in absorption upon addition of pyridine. Arrows indicate areas of increasing and decreasing absorption during the titration; (right) Binding isotherm (black dots) derived from absorption data at $\lambda = 604 - 644$ nm and fit obtained from Origin® (red line).

Run 1:



Run 2:

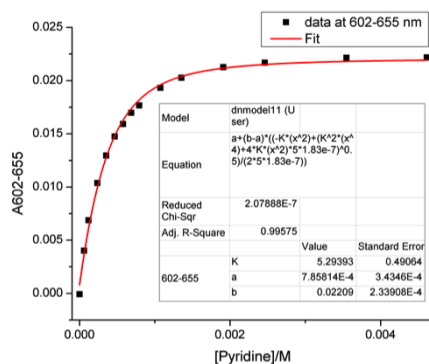
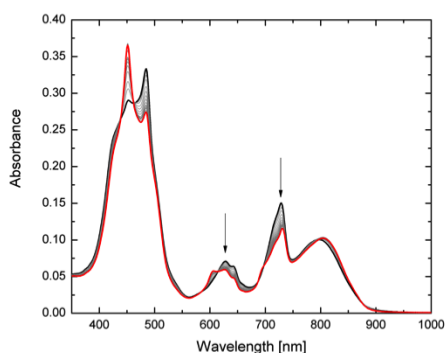
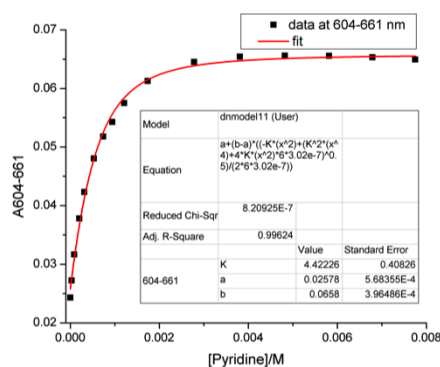
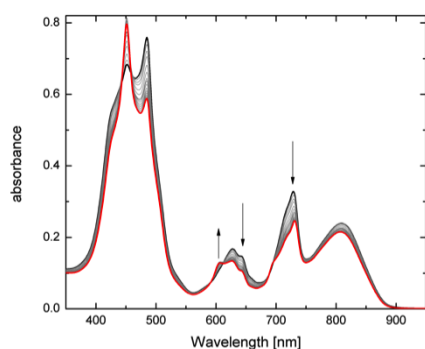


Figure S10 UV/Vis denaturation titration of $(c\text{-P10})_n \bullet (\text{P2py2})_5$ ($[\text{complex}] = 1.83 \times 10^{-7} \text{ M}$) with pyridine in toluene at 298 K (Run 1: $R^2 = 0.997$; Run 2: $R^2 = 0.996$). (left) Changes in absorption upon addition of pyridine. Arrows indicate areas of increasing and decreasing absorption during the titration; (right) Binding isotherm (black dots) derived from absorption data at $\lambda = 602 - 655 \text{ nm}$ and fit obtained from Origin® (red line).

Run 1:



Run 2:

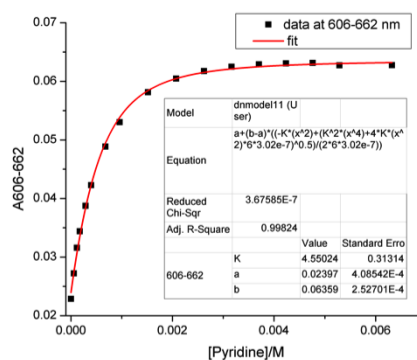
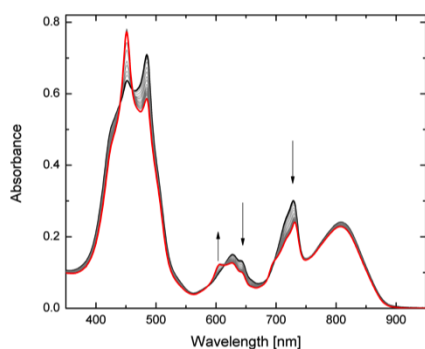
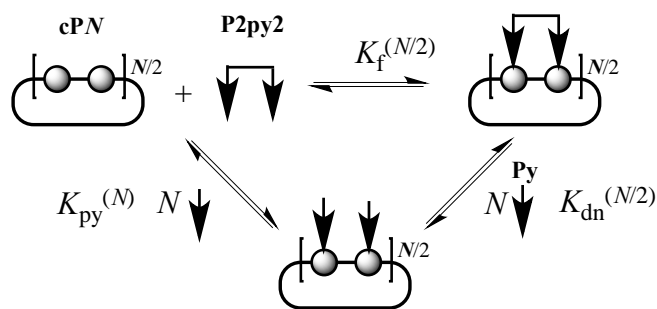


Figure S11 UV/Vis/NIR denaturation titration of $(c\text{-P12})_2(\text{P2py}_2)_6$ ($[\text{complex}] = 3.02 \times 10^{-7} \text{ M}$) with pyridine in toluene at 298 K (Run 1: $R^2 = 0.996$; Run 2: $R^2 = 0.998$). (left) Changes in absorption upon addition of pyridine. Arrows indicate areas of increasing and decreasing absorption during the titration; (right) Binding isotherm (black dots) derived from absorption data at $\lambda = 604 - 661 \text{ nm}$ and fit obtained from Origin[®] (red line).

Calculation of the formation constant K_f



Scheme S2 Generic thermodynamic cycle for the formation of a double strand complex.

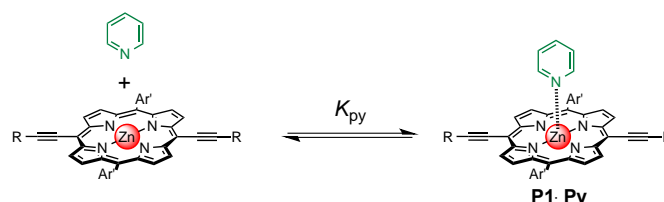
The formation constants K_f for nanoring-dimer complexes were calculated from

$$K_f = \frac{K_{py}^2}{K_{dn}}, \quad (\text{eq. 15})$$

where K_{py} is the formation constant for the binding of pyridine to porphyrin monomer and K_{dn} is the denaturation constant of the nanoring-dimer complexes with pyridine. The calculated values of K_f are listed in Table S2 in Section D4.

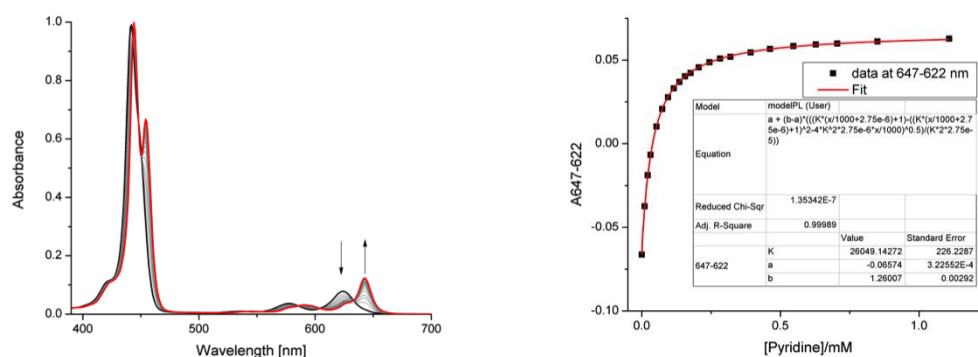
D3. Determination of reference constants

To derive K_f of nanoring-dimer complexes by equation 13, the binding constant of pyridine to porphyrin monomer complex (K_{py}) is needed. It was derived by UV/Vis formation titration of pyridine with porphyrin monomer (Scheme S4).



Scheme S3 Formation of pyridine and porphyrin monomer complex (**P1•Py**). Ar' = 3,5-bis(octyloxy)phenyl, R = trihexylsilyl.

Run 1:



Run 2:

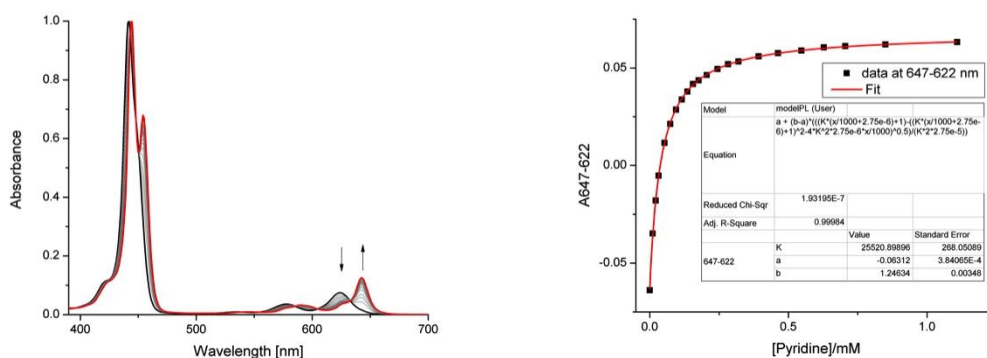
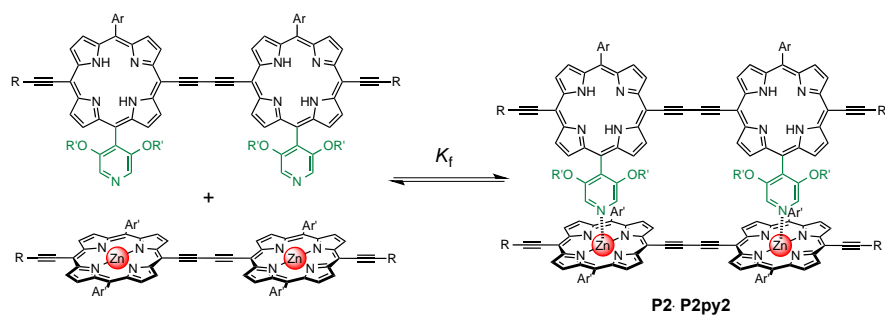


Figure S12 UV/Vis formation titration of **P1** ($[P1] = 2.75 \times 10^{-6}$ M) with pyridine in toluene at 298 K; (Run 1, $R^2 = 0.9999$; Run2, $R^2 = 0.9998$); $K_{py} = (2.58 \pm 0.26) \times 10^4$ M $^{-1}$. (left) Changes in absorption upon addition of pyridine. Arrows indicate areas of increasing and decreasing absorption during the titration; (right) Binding isotherm (black dots) derived from absorbance data at $\lambda = 647 - 622$ nm and fit obtained from Origin[®] (red line).

The empirical data were in excellent agreement with the theoretically derived 1:1 binding equation 10, resulting in to $K_{py} = (2.58 \pm 0.26) \times 10^4$ M $^{-1}$ (Figure S14). Monomer was used instead of the cyclic porphyrin oligomers to model this interaction in order to avoid the initial aggregation of the nanorings during this titration.

Likewise, the binding constant of **P2py2** to porphyrin dimer was also elucidated as a reference in comparison to the binding constants of the family of nanoring-dimer complexes (Scheme S5).



Scheme S4 Formation of **P2py2** and porphyrin dimer complex (**P2•P2py2**).

$Ar = 3,5\text{-bis}(\text{trihexylsilyl})\text{phenyl}$, $Ar' = 3,5\text{-bis}(\text{octyloxy})\text{phenyl}$, $R = \text{trihexylsilyl}$, $R' = \text{dodecyl}$.

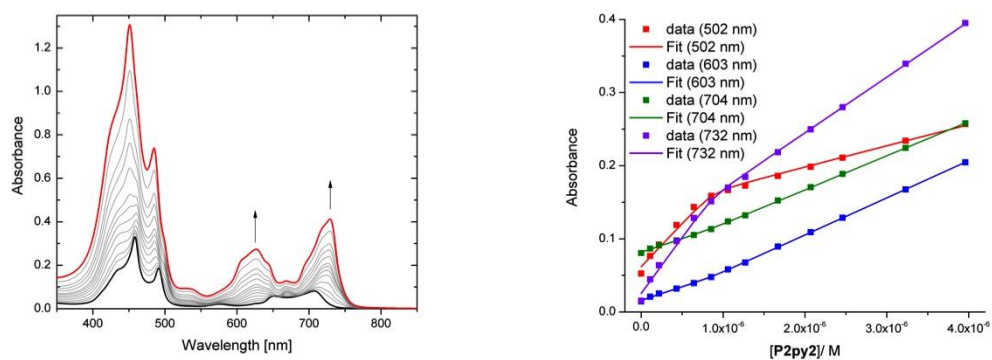
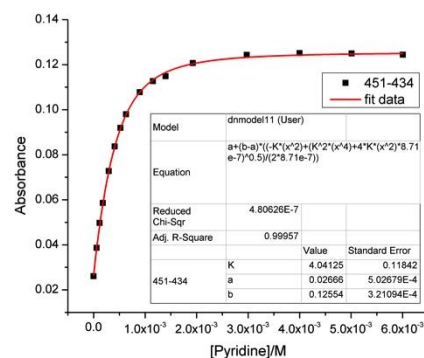
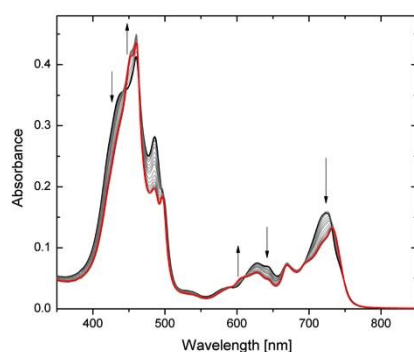


Figure S13 UV/Vis/NIR formation titration of **P2** ($[P2] = 8.71 \times 10^{-7} \text{ M}$) with **P2py2** in toluene at 298 K ($K_f = (1.74 \pm 0.20) \times 10^8 \text{ M}^{-1}$). (left) Changes in absorbance upon addition of **P2py2**. Arrows indicate areas of increasing absorbance during the titration; (right) Binding isotherm (dots) derived from absorbance data at various wavelengths and fit obtained from SPECIFIT® (line). The increment after addition of 1 equivalent of **P2py2** is attributed to the absorbance overlapping between excess **P2py2** and the complex.

Run 1:



Run 2:

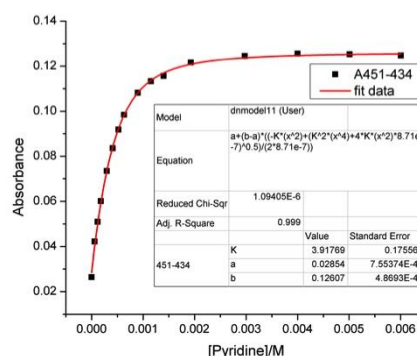
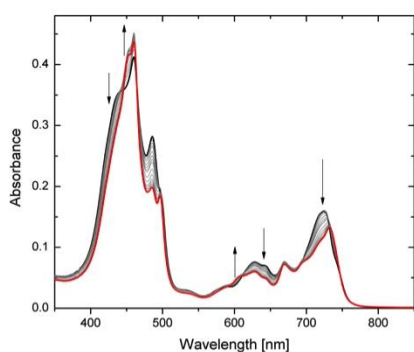


Figure S14 UV/Vis/NIR denaturation titration of **P2•P2py2** ($[complex] = 8.71 \times 10^{-7} M$) with pyridine in toluene at 298 K (Run1: $R^2 = 0.9996$; Run2: $R^2 = 0.999$). (left) Changes in absorption upon addition of pyridine. Arrows indicate areas of increasing and decreasing absorption during the titration; (right) Binding isotherm (black dots) derived from absorption data at $\lambda = 451 - 434$ nm and fit obtained from Origin® (red line).

The binding isotherm of dimer-dimer formation was too sharp and the increment after addition of 1.0 equivalent of dimer due to the overlapping absorption between the complex and excess dimer. This makes the difficulty to obtain a curve fitting a 1:1 model for formation from equation 10 (Figure S15). The first attempt to fit the data using a 1:1 model calculated by SPECIFIT® provided good agreement between the empirical data and simulated data, giving $K_f = (1.74 \pm 0.20) \times 10^8 M^{-1}$. Nevertheless, the binding constant of this complex is too strong ($K_f > 10^7 M^{-1}$). The breakup titration was therefore performed to confirm K_f from SPECIFIT® again and fitted successfully using equation 12 (Figure S16), giving $K_{dn} = 3.98 \pm 0.10 M^{-1}$. $K_f = (1.67 \pm 0.34) \times 10^8 M^{-1}$ was calculated using the thermodynamic cycle (equation 13) and is listed in Table S2. The two values of K_f from SPECIFIT® and from the breakup titration are in good agreement.

D4. Summary of denaturation and formation constants of nanoring-dimer complexes

K_{dn} evaluated by equation 12 and K_f calculated by equation 13 are listed in Table S2. The binding constants for the various sizes of porphyrin nanoring with dimer are compared graphically in Figure S17.

Table S2 Denaturation constants of nanoring-dimer complexes with pyridine and formation constants of nanoring-dimer complexes determined via denaturation titrations

PN	K_{dn}, M^{-1}			K_f, M^{-1}
	Run 1	Run 2	Average	
P2	4.04 ± 0.20	3.92 ± 0.20	3.98 ± 0.14	$(1.67 \pm 0.34) \times 10^8$
c-P6	25.0 ± 1.25	26.0 ± 1.30	25.5 ± 0.90	$(2.60 \pm 0.53) \times 10^7$
c-P8	8.73 ± 0.66	8.23 ± 0.60	8.48 ± 0.45	$(7.82 \pm 1.60) \times 10^7$
c-P10	5.16 ± 0.52	5.29 ± 0.53	5.23 ± 0.37	$(1.27 \pm 0.27) \times 10^8$
c-P12	4.42 ± 0.44	4.55 ± 0.46	4.49 ± 0.32	$(1.48 \pm 0.31) \times 10^8$

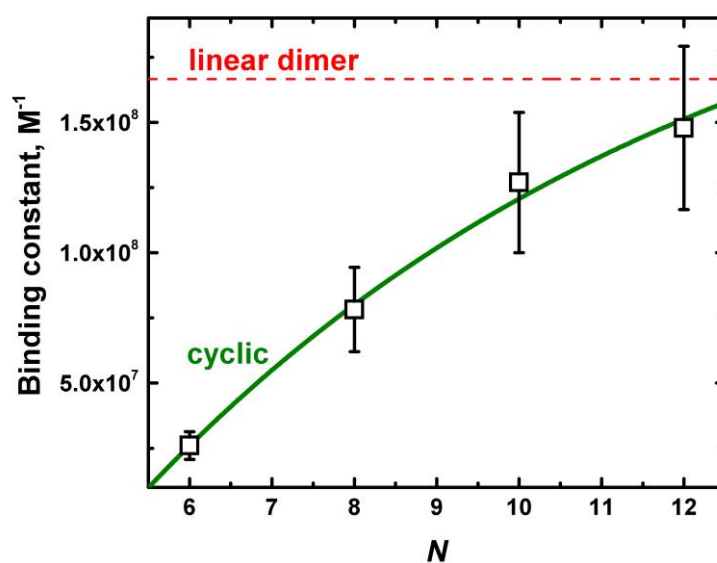


Figure S15 Comparison of the formation constants as a function of ring size.

E. Excitation Wavelength Selection

The excitation wavelength for photoluminescence studies of the nanoring-dimer complex was chosen by analysis of the UV-Vis absorption spectra of the components, as shown in Figure S18. A wavelength of 627 nm was chosen for having the greatest selectivity of the dimer over the nanoring maximizing the yield of excitons formed on the dimer.

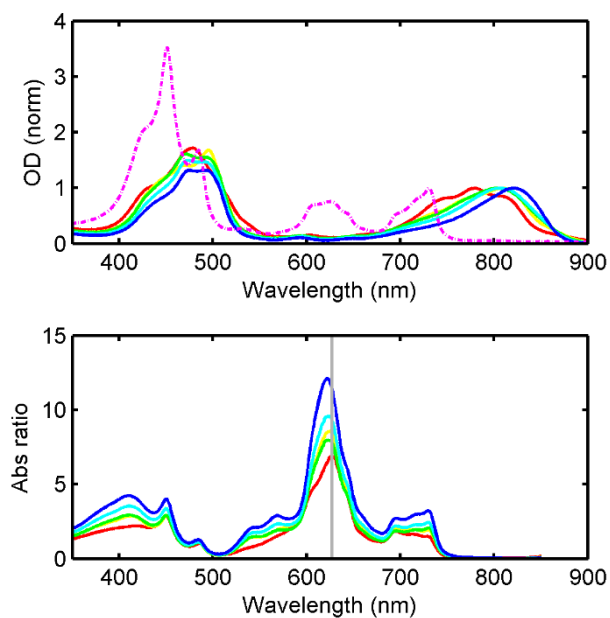


Figure S16 (Upper) the optical density for the dimer (dashed purple line) and each nanoring sample (solid lines, **c-P6** red, **c-P8** yellow, **c-P10** green, **c-P12** cyan and **c-P30** blue) on a scale normalized to the NIR absorption of the nanoring. (Below) the ratio of optical densities for the dimer and nanoring, with higher values indicating more selective excitation of the dimer. The 627 nm excitation chosen is indicated with a vertical grey line.

F. Photoluminescence observation of Complex Dissociation

The photoluminescence quenching technique used in this study requires control over the association state of the complexes. To achieve this, the bound state was first assembled, targeting approximately one dimer per nanoring. After energy transfer was measured, an excess of pyridine (approximately 10% v/v) was added to the solution, which displaced the dimer from the nanoring, effectively dissociating the complex and switching off the energy transfer process. To confirm the dissociation process, photoluminescence spectra were measured immediately before and after the addition of pyridine (for a slight excess of dimers), as shown in Figure S19. It can be seen that upon addition of pyridine, the photoluminescence yield from the dimer (observed between 700 nm and 780 nm) increases, while the emission from the nanoring (observed between 800 nm and 900 nm) decreases and redshifts.

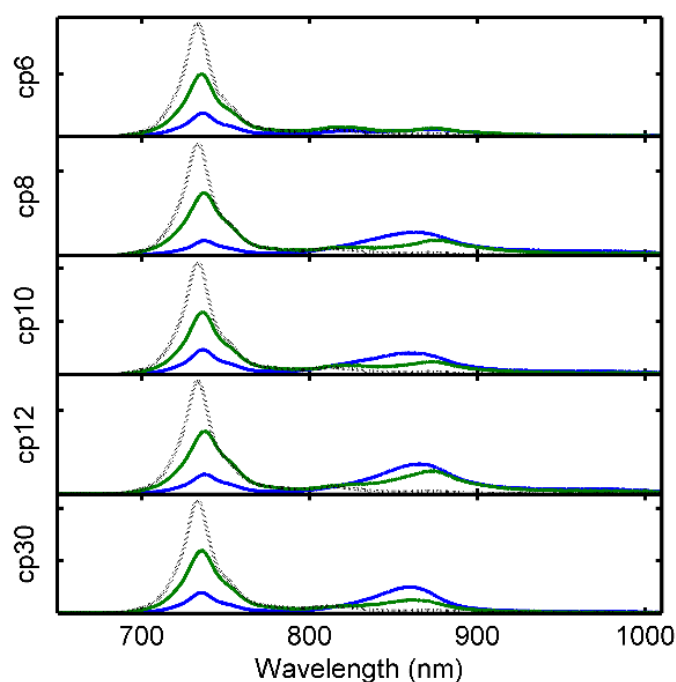


Figure S19 Time-integrated photoluminescence for each nanoring-dimer system, in the assembled (blue) and disassembled state (green), along with the isolated dimer (grey) for reference. Excitation wavelength: 627 nm.

G. Experimental Energy Transfer Rates

By measuring the time-resolved photoluminescence from the dimer in both the associated and dissociated complex state, the energy transfer pathway was isolated. We assume here that the only additional energy quenching pathway in the assembled state is due to energy transfer to the nanoring. By taking the ratio between the emission lifetimes in the two states, a transfer rate is calculated. Because the energy transfer to the nanoring dominates (with a 99.9% drop in dimer quantum yield for the sub-stoichiometric case), a simple comparison of photoluminescence decay rates can be used to confirm that the energy transfer occurs on a near identical timescale for each nanoring acceptor system. This measurement is shown in Figure S20. While all of the decays overlap in the data, a slight change in offset can be observed. This is due to the lower dimer-nanoring binding constant leading to a non-negligible population of unbound dimers for the smaller nanoring case (**c-P6**) as discussed in Reference 8.

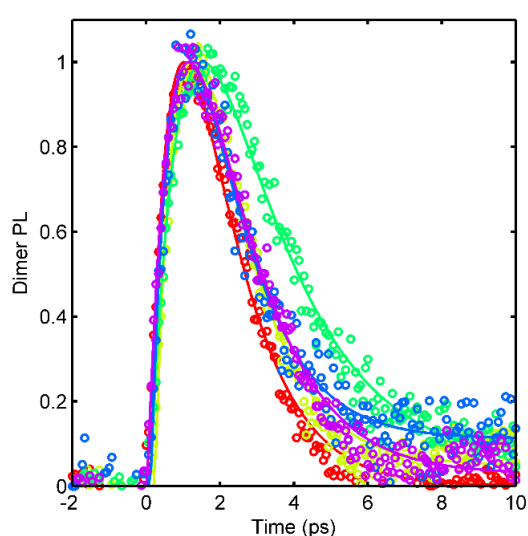


Figure S20: Photoluminescence decay rates for dimer emission to each nanoring acceptor (**c-P6** red, **c-P8** yellow, **c-P10** green, **c-P12** blue and **c-P30** purple). All transfers show identical rise times, and similar decay times.

H. The models of nanorings minimized geometries

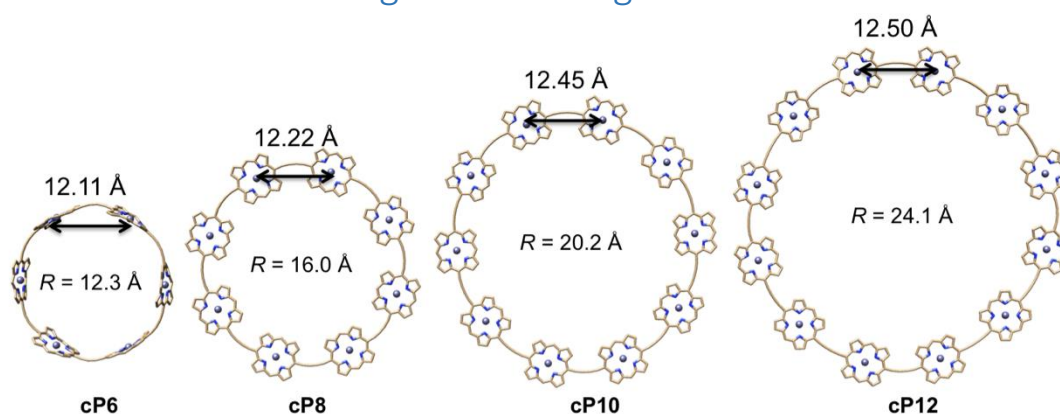


Figure S21: The models of **c-PN** from 6- to 12-rings are energy minimized geometries calculated using MM+ force field in HyperChem®. R is the radius measured to Zn centers.

I. Energy Transfer Models

Energy transfer in supramolecular systems of chromophores has been widely investigated at various levels of theory, typically starting from the traditional Förster point-dipole approach⁹ up to full quantum chemical treatments.¹⁰ For molecules containing up to 30 porphyrin sub-units, high level theory is typically computationally infeasible; however, given the small separation of the donor and acceptor molecules (approximately 10 Å) the point-dipole model is known to be unreliable. For this reason, more pragmatic approaches have been developed, typically based on the division of the transition dipole moments of the donor and acceptor molecules into a number of sub-dipoles (such as in the line-dipole approach¹¹), the inclusion of higher order multipoles, or through use of the transition density cube¹² method. Using these methods to obtain the geometry-determined electronic coupling strength V_{DA} , the theoretical rate of energy transfer (k_{DA}) may then be calculated. These methods typically start from a modified version of Fermi's Golden Rule,¹¹

$$k_{DA} = \frac{2\pi}{\hbar} |V_{DA}|^2 \int_{-\infty}^{\infty} \alpha_A(E) f_D(E) dE \quad (\text{eq. 16})$$

where α_A is the acceptor state absorption spectrum and f_D is the fluorescence spectrum of the donor, both area normalized on an energy scale such that $\int_{-\infty}^{\infty} \alpha dE = \int_{-\infty}^{\infty} f dE = 1$. The latter term is often represented by $I \equiv \int_{-\infty}^{\infty} \alpha_A(E) f_D(E) dE$. The overall transfer rate is determined by both the electronic coupling term and the spectral term; these parameters are shown in Figure 5 of the manuscript.

In general, $V_{DA} = D(V_{coulomb} + \dots)$, where D describes dielectric environment effects, $V_{coulomb}$ contains dipole and higher order Coulombic (free-space) terms, and further terms contain through-bond and short-range effects. These latter effects are neglected here due to the small orbital overlaps between the antenna and nanoring molecules. In the original Förster formulation, $D = 1/n^2$ (where n is the refractive index of the solvent), $V_{coulomb}$ is truncated at the dipole term, and the approximation of the transition dipole moments of the donor and acceptor molecules as point-dipoles is used.^{9,13} Herein, a value of $n = 1.481$ is used for the dielectric environment of toluene solvent.¹⁴ This treatment leads to a coupling strength V_{PDM} , given by

$$V_{PDM} = \frac{1}{4\pi\epsilon_0} |\mu_D| |\mu_A| \frac{\kappa_{DA}}{|R_{DA}|^3} \quad (\text{eq. 17})$$

Where μ_x is the transition dipole moment for the donor ($x = D$) or acceptor ($x = A$), κ_{DA} is a geometrical term, and R_{DA} is the spatial separation of the two point dipoles.

The transition dipole strengths are calculated from the experimental data for the donor as

$$\mu_D^2 = \frac{\varphi 3\epsilon_0 \hbar c^3}{\tau 2\omega_{D,0}^3} \quad (\text{eq. 18})$$

Where φ is the quantum efficiency of the transition, τ is the measured lifetime of the excited state in isolation, and $\omega_{D,0}$ is the mean angular frequency of the transition.¹⁵ The transition dipole moment for the acceptor is given by

$$\mu_A^2 = \frac{3\sigma\epsilon_0 \hbar c}{\pi\omega_{A,0}} \quad (\text{eq. 19})$$

where σ is the absorbing state cross-sectional area and $\omega_{A,0}$ is the mean angular frequency of the transition.¹⁵ It is noted that while the transition dipole moment of the donor is easily defined from

experimental values, the value for the dipole moment of the acceptor can be more challenging to determine.

For the point-dipole model described in the main text (Model 1), the electronic coupling V_{DA} shown in Figure 5 is calculated by combining the equations 15, 16 and 17.

In the line-dipole model, the Förster approach is extended to distribute the transition dipole strength of both the donor and acceptor dipoles over sub-dipoles throughout the molecule. This approach has been shown to provide a significant improvement over the point-dipole approach, particularly for small donor-acceptor separations.¹¹ In this case, the coupling strength can be written as

$$V_{LDM} = \frac{1}{4\pi\epsilon_0} \sum_{a,d} \left(\frac{|\mu_A^{(a)}||\mu_D^{(d)}|}{|R_{a,d}|^3} \times \kappa_{a,d} \right) \quad (\text{eq. 20})$$

The acceptor and donor sub-dipoles $\mu_A^{(a)}$ and $\mu_D^{(d)}$ are indexed by a and d , respectively, and $R_{a,d}$ is the vector connecting the indexed donor and acceptor sub-dipoles. The relative strengths of each sub-dipole may be expressed as a scalar coefficient Ψ , such that $\mu_A^{(a)} = \Psi_A(a)\mu_A$. The sub-dipole strengths are normalised such that $\sum_a \Psi_A(a) = 1$. The dipole strength is distributed amongst the sub-dipoles in two ways; in the case of the donor dimer and the localised acceptor states, the coefficients follow a sinusoidal distribution with the ‘excitonic center-of-mass’ at the middle of the dimer,¹¹ such that

$$\Psi_D(d) = \frac{\sin(\pi d/l_d)}{\sum_d \sin(\pi d/l_d)} \quad (\text{eq. 21})$$

where, l_d is the total number of donor sub-dipoles. The spatial arrangement of exciton strength for the delocalised states on the acceptor nanoring depends on which one of the non-degenerate energy states we consider to be the acceptor state, known as the k -state.

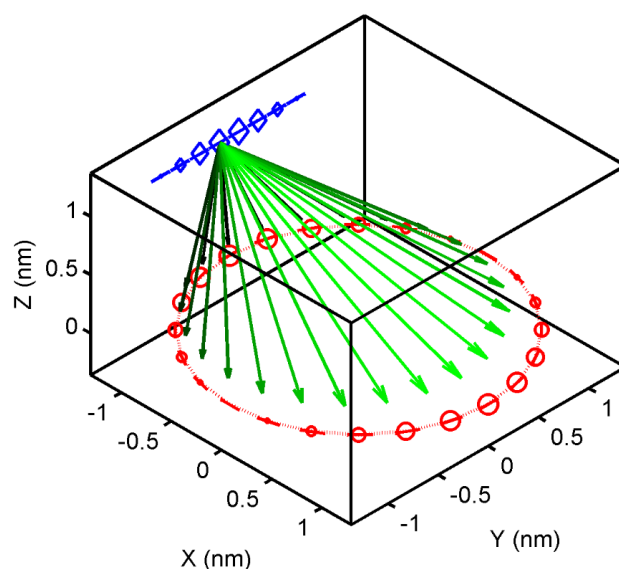


Figure S22 Schematic representation of energy transfer from the donor dimer (blue) to the fully delocalized $k=1$ state of the c-P6 nanoring (red) in the line-dipole framework. The marker size represents the local dipole strength of that sub-unit, while the arrow colors vary from black to green with decreasing strength of the dipole element.

By simplifying the nanoring as a perfect cyclic array of n identical chromophores, we can describe excitons on arrays of n chromophores using either localized or delocalized basis states.¹⁶ In the localized basis, $|n = x\rangle$ represents an exciton completely localized on a single chromophore x ; all $|n\rangle$ states have the same energy. Conversely, delocalized states may be described by $|k\rangle$, effectively a Frenkel representation of the exciton wave-function,

$$|k\rangle = \frac{1}{\sqrt{N}} \sum_{n=1}^N \exp(2\pi i k n / N) |n\rangle \quad (\text{eq. 22})$$

The index k runs from 0 to $N/2$, where N is the number of possible localized states; contrary to the localized states, $|k\rangle$ states are not energetically degenerate. The far-field dipole strength for each molecular exciton state can be calculated by summation of the sub-dipoles; it has been shown that for all except the $k=1$ state, this dipole is negligible – the other states are ‘optically dark’ in the absence of disorder.

We consider three situations; (Model 1) the point dipole model, with donor and acceptor dipoles pinned at the center of their respective moieties, (Model 2) where the $k = 1$ state remains the sole optically active state (as depicted in Figure S22), and finally (Model 3) where the strain induced by dimer bonding modifies the local energy of the attached porphyrin ring to create a localized state as described in the manuscript. The model, written in MATLAB, performs as:

1. **Generate a nanoring-dimer complex:** this is assumed to be an ideal circular nanoring, with equally spaced porphyrin units. The porphyrin-porphyrin separation used is 12.11 Å, 12.22 Å, 12.45 Å, 12.50 Å and 12.50 Å for 6, 8, 10, 12 and 30 unit nanorings, respectively (see Figure S21). These values are calculated from energy minimized HyperChem modeling. The dimer-nanoring spacing is given as 10.16 Å, and the dimer porphyrin separation is 13.5 Å throughout, as previously determined (see Supporting Information to Reference 8).
2. **Distribute sub-dipoles as appropriate:** For the point-dipole model, the dipole is pinned at the center of the molecule. For line-dipole models, the dipole strength is distributed over 6 sub-dipoles per porphyrin unit – increasing the number of sub-dipole did not alter the numerical result of the calculation.
3. **Calculate the total dipole strength:** The emitting dipole strength was calculated using values for the quantum efficiency and lifetime obtained from standard spectroscopic measurements as described in Reference 17.
4. **Calculate the energy coupling:** The energy coupling is calculated using either the point dipole model (Eqn. 15) for Models 1, or the line-dipole model (Eqn. 18) for Models 2 and 3, respectively. The parameters R and κ are obtained from the geometrical model described in step 1.
5. **Calculate the spectral coupling:** The spectral coupling is calculated using the fluorescence shape of isolated free-base dimer, and the absorbing state spectrum as shown in Eqn. 14. For Models 1 and 2, the far-field spectrum of the nanoring obtained by UV-Vis-NIR spectroscopy is used. For the localized absorbing state, the spectrum of an $N = 6$ linear oligomer attached to a **T6** template was used. This is chosen as representative of the geometrically confined, bent and torsionally locked component of the nanoring immediately below the dimer. The molar absorptivity data for a series of linear oligomers bound to a cyclic template is shown in Figure S23 as reported by Hogben *et al.*¹⁸ These oligomer systems were chosen as most representative of the bent localized excitonic state below the antenna molecule. The templates are all based on **T6**, but with spokes removed where required. While the bending angle will be related to the nanoring size to a degree, the suppressed torsional motion is effectively represented.

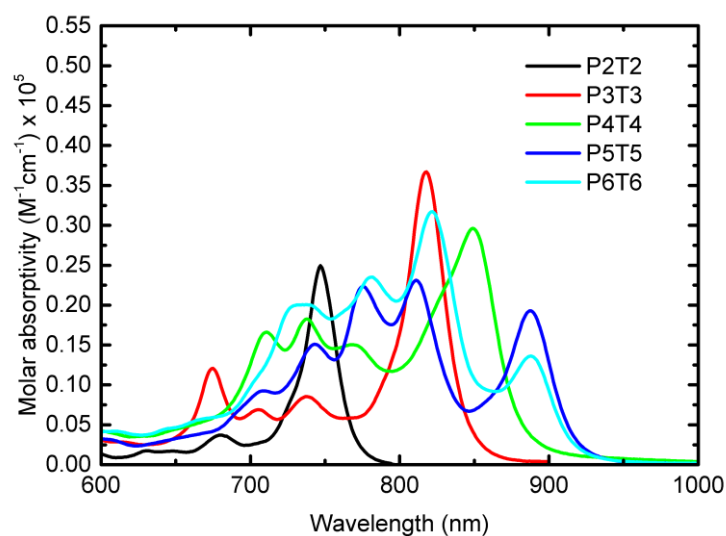


Figure S23: Experimentally determined absorption coefficients for linear oligomers on a template.

Figure S24 shows how the modeled energy transfer rate varies with acceptor state size assuming a **P2**, **P3**, **P4**, **P5** and **P6**-like acceptor state.

6. **Calculate energy transfer rate:** The effective energy transfer rate is then calculated for the given model and acceptor species.

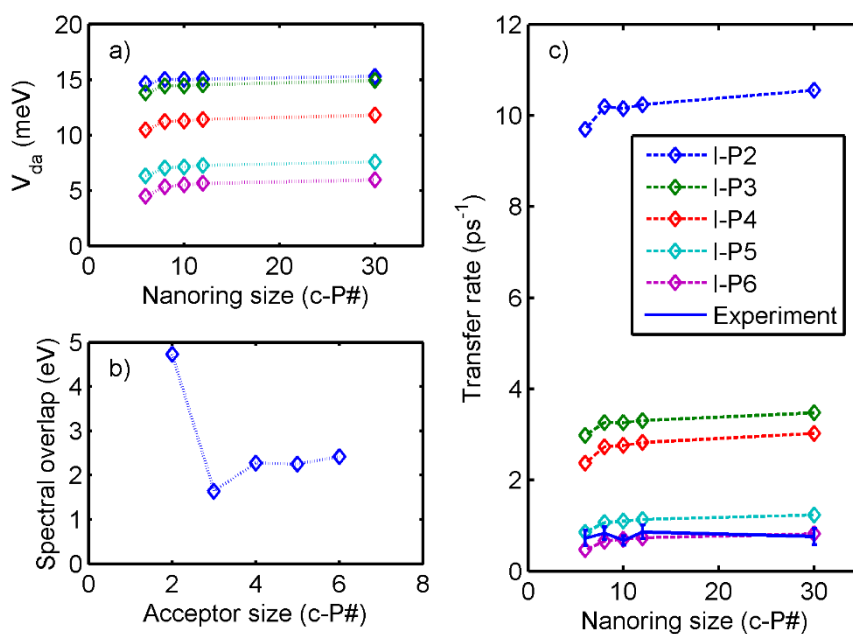


Figure S24: Calculation of a) coupling, b) spectral overlap and c) overall transfer rate for different choices of acceptor state. Each acceptor state is described by a distribution of dipole strength, and a molar extinction spectrum, where the latter is taken from experimental data for Zn porphyrin oligomers on template as described in the text. The experimental results match most closely to energy transfer to a linear 6-porphyrin acceptor state, used for the modeling.

References

- (1) Hoffmann, M.; Kärnbratt, J.; Chang, M.-H.; Herz, L. M.; Albinsson, B.; Anderson, H. L. Enhanced π Conjugation around a Porphyrin[6] Nanoring. *Angew. Chemie Int. Ed.* **2008**, *47*, 4993–4996.
- (2) Hoffmann, M.; Wilson, C. J.; Odell, B.; Anderson, H. L. Template-Directed Synthesis of a π -Conjugated Porphyrin Nanoring. *Angew. Chemie Int. Ed.* **2007**, *46*, 3122–3125.
- (3) O'Sullivan, M. C.; Sprafke, J. K.; Kondratuk, D. V.; Rinfrey, C.; Claridge, T. D. W.; Saywell, A.; Blunt, M. O.; O'Shea, J. N.; Beton, P. H.; Malfois, M.; Anderson, H. L. Vernier Templating and Synthesis of a 12-Porphyrin Nano-Ring. *Nature* **2011**, *469*, 72–75.
- (4) Liu, S.; Kondratuk, D. V.; Rousseaux, S. A. L.; Gil-Ramírez, G.; O'Sullivan, M. C.; Cremers, J.; Claridge, T. D. W.; Anderson, H. L. Caterpillar Track Complexes in Template-Directed Synthesis and Correlated Molecular Motion. *Angew. Chemie Int. Ed.* **2015**, *54*, 5355–5359.
- (5) Gaefke, G.; Höger, S. [(3-Cyanopropyl)diisopropylsilyl]acetylene, a More Stable Analogue of [(3-Cyanopropyl)dimethylsilyl]acetylene. *Synthesis (Stuttg.)* **2008**, *2008*, 2155–2157.
- (6) Kiriya, D.; Chang, H.-C.; Kitagawa, S. Molecule-Based Valence Tautomeric Bistability Synchronized with a Macroscopic Crystal-Melt Phase Transition. *J. Am. Chem. Soc.* **2008**, *130*, 5515–5522.
- (7) Féau, C.; Klein, E.; Kerth, P.; Lebeau, L. Preparation and Optical Properties of Novel 3-Alkoxy-carbonyl Aza- and Diazocoumarins. *Synth. Commun.* **2010**, *40*, 3033–3045.
- (8) Parkinson, P.; Knappke, C. E. I.; Kamonsutthipaijit, N.; Sirithip, K.; Matichak, J. D.; Anderson, H. L.; Herz, L. M. Ultrafast Energy Transfer in Biomimetic Multistrand Nanorings. *J. Am. Chem. Soc.* **2014**, *136*, 8217–8220.
- (9) Förster, T. Zwischenmolekulare Energiewanderung Und Fluoreszenz. *Ann. Phys.* **1948**, *437*, 55–75.
- (10) Beljonne, D.; Curutchet, C.; Scholes, G. D.; Silbey, R. J. Beyond Förster Resonance Energy Transfer in Biological and Nanoscale Systems. *J. Phys. Chem. B* **2009**, *113*, 6583–6599.
- (11) Beenken, W. J. D.; Pullerits, T. Excitonic Coupling in Polythiophenes: Comparison of Different Calculation Methods. *J. Chem. Phys.* **2004**, *120*, 2490.
- (12) Krueger, B. P.; Scholes, G. D.; Fleming, G. R. Calculation of Couplings and Energy-Transfer Pathways between the Pigments of LH2 by the Ab Initio Transition Density Cube Method. *J. Phys. Chem. B* **1998**, *102*, 5378–5386.
- (13) Scholes, G. D. Long-Range Resonance Energy Transfer in Molecular Systems. *Annu. Rev. Phys. Chem.* **2003**, *54*, 57–87.
- (14) Kedenburg, S.; Vieweg, M.; Gissibl, T.; Giessen, H. Linear Refractive Index and Absorption Measurements of Nonlinear Optical Liquids in the Visible and near-Infrared Spectral Region. *Opt. Mater. Express* **2012**, *2*, 1588.
- (15) Hilborn, R. C. Einstein Coefficients, Cross Sections, F Values, Dipole Moments, and All That. *Am. J. Phys.* **1982**, *50*, 982–986.
- (16) Cogdell, R. J.; Gall, A.; Köhler, J. The Architecture and Function of the Light-Harvesting Apparatus of Purple Bacteria: From Single Molecules to in Vivo Membranes. *Q. Rev. Biophys.* **2006**, *39*, 227–324.
- (17) Anderson, H. L.; Martin, S. J.; Bradley, D. D. C. Synthesis and Third-Order Nonlinear Optical

- Properties of a Conjugated Porphyrin Polymer. *Angew. Chemie Int. Ed. English* **1994**, *33*, 655–657.
- (18) Hogben, H. J.; Sprafke, J. K.; Hoffmann, M.; Pawlicki, M.; Anderson, H. L. Stepwise Effective Molarities in Porphyrin Oligomer Complexes: Preorganization Results in Exceptionally Strong Chelate Cooperativity. *J. Am. Chem. Soc.* **2011**, *133*, 20962–20969.